JOURNAL OF GEOPHYSICAL RESEARCH, VOL. 108, NO. B10, 2507, doi:10.1029/2002JB002072, 2003

***Correction published 19 December 2003***

# Basin-centered asperities in great subduction zone earthquakes: A link between slip, subsidence, and subduction erosion?

Ray E. Wells and Richard J. Blakely
U.S. Geological Survey, Menlo Park, California, USA

Yuichi Sugiyama
Geological Survey of Japan, National Institute of Advanced Industrial Science and Technology, Tsukuba, Ibaraki, Japan

David W. Scholl and Philip A. Dinterman
U.S. Geological Survey, Menlo Park, California, USA

Received 4 July 2002; revised 25 May 2003; accepted 15 July 2003; published 29 October 2003.

[1] Published areas of high coseismic slip, or asperities, for 29 of the largest Circum-Pacific megathrust earthquakes are compared to forearc structure revealed by satellite free-air gravity, bathymetry, and seismic profiling. On average, 71% of an earthquake's seismic moment and 79% of its asperity area occur beneath the prominent gravity low outlining the deep-sea terrace; 57% of an earthquake's asperity area, on average, occurs beneath the forearc basins that lie within the deep-sea terrace. In SW Japan, slip in the 1923, 1944, 1946, and 1968 earthquakes was largely centered beneath five forearc basins whose landward edge overlies the 350°C isotherm on the plate boundary, the inferred downdip limit of the locked zone. Basin-centered coseismic slip also occurred along the Aleutian, Mexico, Peru, and Chile subduction zones but was ambiguous for the great 1964 Alaska earthquake. Beneath intrabasin structural highs, seismic slip tends to be lower, possibly due to higher temperatures and fluid pressures. Kilometers of late Cenozoic subsidence and crustal thinning above some of the source zones are indicated by seismic profiling and drilling and are thought to be caused by basal subduction erosion. The deep-sea terraces and basins may evolve not just by growth of the outer arc high but also by interseismic subsidence not recovered during earthquakes. Basin-centered asperities could indicate a link between subsidence, subduction erosion, and seismogenesis. Whatever the cause, forearc basins may be useful indicators of long-term seismic moment release. The source zone for Cascadia's 1700 A.D. earthquake contains five large, basin-centered gravity lows that may indicate potential asperities at depth. The gravity gradient marking the inferred downdip limit to large coseismic slip lies offshore, except in northwestern Washington, where the low extends landward beneath the coast. Transverse gravity highs between the basins suggest that the margin is seismically segmented and could produce a variety of large earthquakes. *INDEX TERMS:* 7230 Seismology: Seismicity and seismotectonics; 7223 Seismology: Seismic hazard assessment and prediction; 8105 Tectonophysics: Continental margins and sedimentary basins (1212); 8150 Tectonophysics: Plate boundary—general (3040); 1219 Geodesy and Gravity: Local gravity anomalies and crustal structure; *KEYWORDS:* earthquake, subduction, forearc basin, coseismic slip, asperities, gravity, bathymetry, subsidence, subduction erosion

**Citation:** Wells, R. E., R. J. Blakely, Y. Sugiyama, D. W. Scholl, and P. A. Dinterman, Basin-centered asperities in great subduction zone earthquakes: A link between slip, subsidence, and subduction erosion?, *J. Geophys. Res.*, *108*(B10), 2507, doi:10.1029/2002JB002072, 2003.

## 1. Introduction

[2] The world's largest earthquakes (e.g., 1960 Chile $M_w$ 9.5; 1964 Alaska $M_w$ 9.2) occur along subduction zones where oceanic plates are thrust beneath adjacent continents and island arcs (Figure 1). Inversions of seismic, geodetic, and tsunami waveforms for great earthquakes indicate that coseismic slip on the plate boundary thrust is usually nonuniform and contains regions of higher slip or seismic moment release commonly known as asperities [e.g., *Lay and Kanamori*, 1981]. There is some debate about whether asperities represent characteristic geologic features that control the rupture process or rather represent the filling of seismic gaps in a dynamic process [*Thatcher*, 1990; *Scholz*, 1990]. Geologic candidates for asperities include

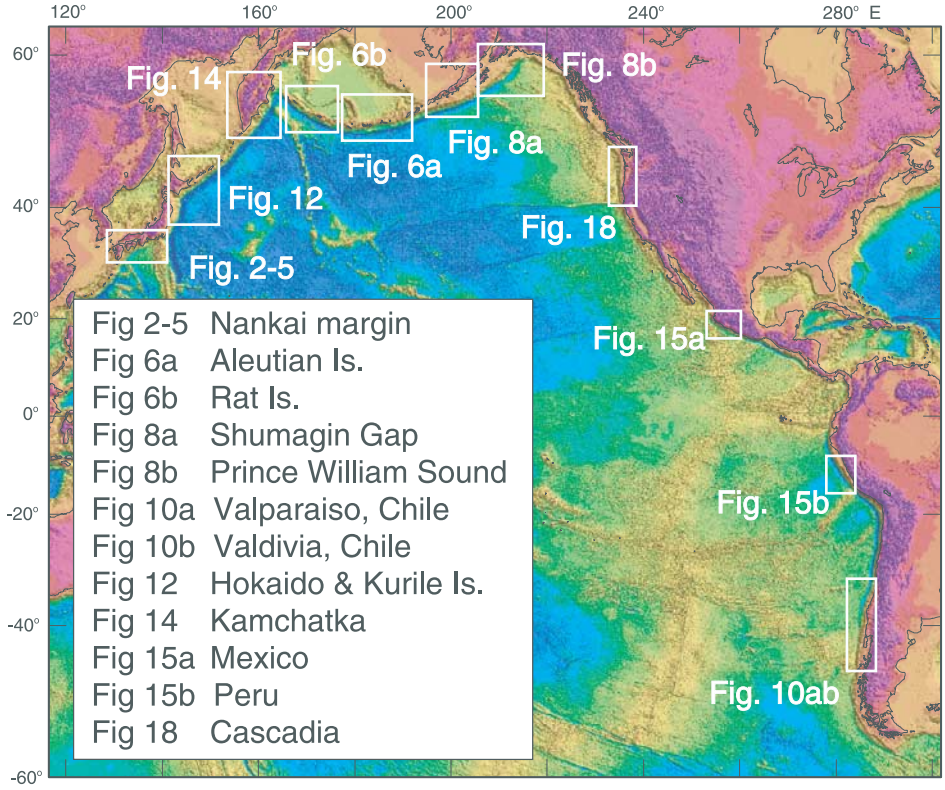


**Figure 1.** Subduction zone study areas and figure locations.

strong crust in the upper plate [e.g., *Byrne et al.*, 1988; *Beck and Christensen*, 1991; *Ryan and Scholl*, 1993], subducted seamounts [*Cloos*, 1992; *Cloos and Shreve*, 1994], or large, smooth surfaces created by subducted sediment [*Ruff*, 1989]. Some have argued that successive large earthquakes within a given fault segment, e.g., the 1957–1986–1996 sequence along the Andreanof segment of the Aleutian arc [e.g., *Boyd et al.*, 1995; *Schwartz*, 1999], have not ruptured the same source region, and that stress transfer and other dynamic processes may be responsible for the earthquake sequence. There is evidence to support both arguments, and one's point of view may depend in part on the scale and resolution of the observations. In great earthquakes, the rupture may reach 1000 km in length, sample the width of the seismogenic zone, and produce large asperities with up to tens of meters of slip. Structures potentially correlative with these asperities should be recognizable in the large-scale architecture of the forearc.

[3] Some asperities appear to persist from one seismic cycle to the next. GPS data from Japan and southern Alaska indicate that centers of slip in previous great earthquakes are now preferentially accumulating strain [*Sagiya*, 1999; *Sagiya et al.*, 2000; *Freymueller et al.*, 2000; *Zweck et al.*, 2002]. Along the Nankai subduction zone of SW Japan (Figure 2), some of the locked patches and high-slip regions appear to correlate with offshore basins, and history suggests that the source regions have persisted over many seismic cycles [*Ando*, 1975; *Sugiyama*, 1994; *Ishibashi and Satake*, 1998]. *Mogi* [1969] recognized that the aftershocks of the 1944 Tonankai and 1946 Nankai earthquakes coincided with offshore depressions, and *Ando* [1975] showed that the 1944 and 1946 source zones as determined from geodetic inversions were essentially centered beneath offshore forearc basins.

[4] The forearc basins may simply indicate strong forearc crust at depth, with passive basin fill trapped behind the growing accretionary prism [*Byrne et al.*, 1988]. Alternatively, *Mogi* [1969] suggested that the downward motion of the lower plate during earthquakes created the depression overlying the rupture zone. *Sugiyama* [1994] considered the basins in part to be the product of cumulative interseismic subsidence not recovered during earthquakes. Although long-term subsidence of the forearc could result from sediment loading or cooling of the forearc [*Dickinson*, 1995], permanent interseismic subsidence might also contribute to the formation of the deep-sea terrace above the source zone. In some subduction zones, kilometer-scale subsidence of the deep-sea terrace and its basins is well documented and is thought to result from basal subduction erosion of the forearc [*von Huene and Scholl*, 1991]. If sustained subsidence of the forearc is spatially related to focused slip beneath offshore depressions, it could indicate a potential link between subsidence, subduction erosion, and seismogenesis.

[5] In this paper, we compile coseismic slip inversions for many of the largest Circum-Pacific subduction zone earthquakes and compare them to forearc structure derived from satellite gravity, seismic profiling, and deep ocean drilling. We attempt to quantitatively test the idea that seismic slip is focused beneath the deep-sea terrace and its basins. We then examine evidence for colocation of large seismic slip and sustained forearc subsidence and consider whether subduction erosion may be linked to the earthquake process. Finally, we use the observed empirical relationship between

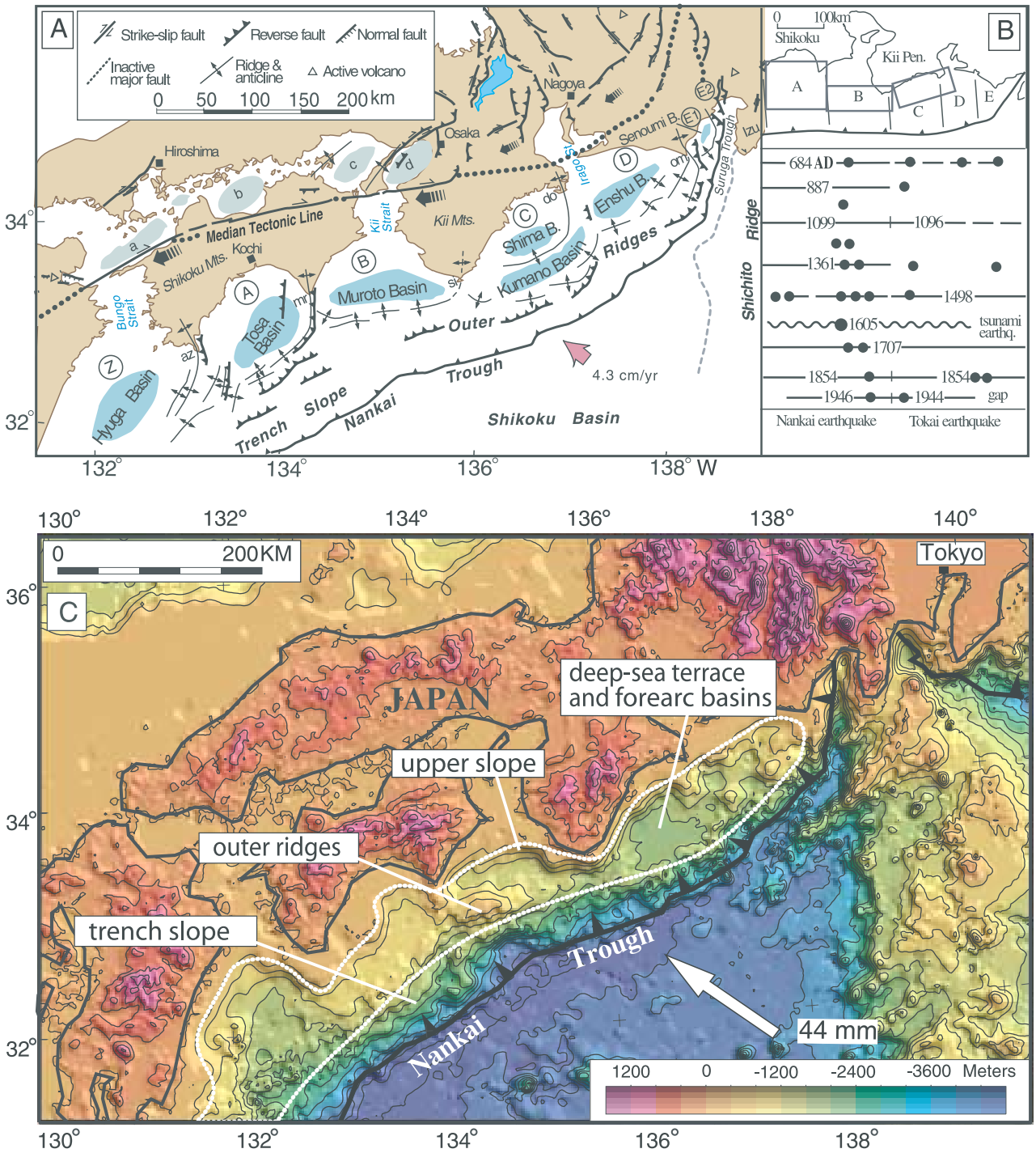


**Figure 2.** (a) Tectonic segments, SW Japan [after *Sugiyama*, 1994]. Oblique subduction of Philippine Sea plate creates offshore marginal basins separated by transverse-faulted anticlines and uplifted headlands: az, Capes Ashizuri; mr, Muroto; si, Shio; do, Daio; om, Omae. (b) The 1300-year history of subduction zone earthquake rupture matches tectonic segments. Solid circles indicate archeological or historical evidence for shaking [*Ishibashi and Satake*, 1998]. Projected fault slip areas (rectangles) for 1944 and 1946 events are centered on offshore basins [*Ando*, 1975]. (c) Physiography of SW Japan from *Smith and Sandwell* [1997], showing large-scale features of the continental slope, deep-sea terrace, and its basins.

slip and crustal structure to predict the distribution of long-term seismic slip on the Cascadia subduction zone, which last ruptured in a great earthquake in 1700 A.D.

## 2. Approach and Definitions

[6] We have compiled published rupture zones and asperities for 29 great ($M_w \geq 8$) and very large ($M_w \geq 7.5$) Circum-Pacific megathrust earthquakes and compared them to subduction zone structure and morphology determined from satellite gravity and bathymetry (Figure 1). Formal slip inversions of seismic, tsunami, and/or geodetic waveforms are available for 20 of the largest historical earthquakes, and seismic source time functions provide areas of greatest moment release for an additional nine (references in Table 1); together they comprise about 7500 km of rupture length. The slip distributions vary greatly in resolution and uncertainties due to the predominantly offshore sources, imperfect receiver arrays, and necessary model assumptions. The most reliable events have slip inversions derived from geodetic, tsunami, and seismic data, as at Nankai and Alaska [e.g., *Satake*, 1993; *Sagiya and Thatcher*, 1999; *Wald and Somerville*, 1995; *Johnson et al.*, 1996]. Slip contours, subfaults, and maximum moment release areas were digitized from the original sources, and the width of the seismogenic zones were determined from the slip distributions, aftershocks, and/or thermal models. Seismic slip areas were calculated, and relative moment distributions were determined assuming constant rigidity. The percentage of the asperity area (the area of maximum defined slip or moment) and seismic moment that occurs beneath the deep-sea terrace and its basins (described below) were compiled for each earthquake and for the Circum-Pacific region (Table 1).

[7] The structure of the continental slope, deep-sea terrace, and basins above the seismogenic zone is derived from satellite bathymetry and free-air gravity of *Smith and Sandwell* [1997]. The terrace and its basins form a well-defined geomorphic feature along most of the subduction zones we studied (see Nankai example, Figure 2). A prominent free-air gravity low, here called the deep-sea terrace low (DSTL), follows the physiographic slope and its basins (Figure 3). Free-air gravity of the continental margin is primarily a function of the bathymetry, but it also includes the effects of low-density sediments filling marginal basins and thinner crust of the forearc. Gravity is particularly useful in highlighting filled forearc basins in areas of high sedimentation rate (e.g., Alaska, south Chile, Cascadia, and SW Japan). The boundaries of the DSTL are mapped with the aid of an algorithm that automatically picks the maximum gravity gradients along the margin [*Blakely and Simpson*, 1986]. An example of the gradients ("maxspots") that outline the DSTL is shown in Figure 3b, but for the sake of clarity, the DSTL boundary in most figures is simply shown as a dotted line. Seismic refraction and reflection profiles across each margin constrain the mapping of sediment-filled forearc basins within the DSTL and confirm the existence of thinner arc crust beneath the slope terrace. The structures we have studied are generally large in lateral dimensions and produce free-air anomalies much larger than the uncertainties of 3–7 mGal in gravity and 20–30 km in spatial resolution characteristic of satellite data [e.g., *Yale et al.*, 1998]. Our quantitative comparison of satellite free-air anomalies with ship-borne data from offshore Washington and Oregon yields similar results, giving us additional confidence in our interpretations based solely on satellite gravity.

[8] The subduction zone study areas are divided into two types following the classification of *von Huene and Scholl* [1991]. The Nankai Trough, Aleutian Islands, southern Alaska, southern Chile, and Cascadia margins are accretionary, where offscraped lower plate sediments form an accretionary prism on the leading edge of the upper plate. Accretionary margins make up about half of the global subduction zone length, and forearc basins inboard of the accretionary prism are floored by arc or continental crust [e.g., *Scholl et al.*, 1987; *Snavely*, 1987; *Parsons et al.*, 1998; *Flueh et al.*, 1998; *Kodaira et al.*, 2000; *Nakanishi et al.*, 2002]. At nonaccretionary margins, including NE Japan, Kurile Islands, Kamchatka, Mexico, and Peru, nearly all the sediment is subducted beneath a forearc consisting of a thinned wedge of continental or arc crust extending nearly to the trench [*Tsuru et al.*, 2000; *Klaeschen et al.*, 1994; *von Huene et al.*, 1994; *von Huene and Lallemand*, 1990]. The nonaccretionary margins provide good geologic evidence for sustained subsidence above the source region and basal subduction erosion of the forearc [e.g., *von Huene and Scholl*, 1991].

## 3. Earthquakes at Accretionary Margins

### 3.1. SW Japan

[9] On the satellite gravity map of the Nankai margin, the forearc basins show up as pronounced gravity lows (compare Figures 2a and 3a). They are separated by transverse highs marking the seaward plunging anticlinal uplifts at each coastal promontory. Seismic profiles across the source regions of the great 1944 and 1946 earthquakes (Figures 4a and 4b) show that thinned arc crust extends beneath the basins almost to the outer arc high [*Nakanishi et al.*, 2002; *Kodaira et al.*, 2000]. The epicenters of the major earthquakes tend to lie on the pronounced gravity gradients along the transverse structure (Figure 3a). However, the most striking correlation exists between the gradient marking the landward limit of the basins and the 350°C isotherm [*Hyndman and Wang*, 1995b], presumably marking the downdip limit of locking and stick-slip behavior on the plate boundary (Figure 3b).

[10] *Sagiya and Thatcher* [1999] have reexamined the distribution of combined slip during the 1944 Tonankai and 1946 Nankaido thrust earthquakes along the Nankai trough. Their inversion combines leveling, triangulation, and tide gauge data with earlier results from tsunami waveform models [*Satake*, 1993] and corrections for the effect of splay faults and interseismic deformation. When plotted on the gravity map (Figure 5a), coseismic slip on the plate boundary thrust of up to 6 m is concentrated in oval-shaped patches that mimic the location and trend of the Tosa, Muroto, and Shima basins (basins A–C of *Sugiyama* [1994]) (Figure 2). Up to 3 m of slip also occurred beneath the gravity highs of Cape Muroto and the Kii Mountains. Reanalysis of the tsunami data using more detailed bathymetry and fault models (Figure 5b) confirms this general pattern [*Tanioka and Satake*, 2001a, 2001b] but suggests

**Table 1.** Slip Distributions and Asperities for Some Great and Very Large Subduction Zone Earthquakes[a]

| Date | Location | $M_w$ | Slip or Moment Inversion | DSTL Area/Total Slip Area Percentage | Seismic Moment Percentage in DSTL | Asperity Area Percentage in DSTL | Asperity Area Percentage Under Basins | Basin Area/Total Slip Area Percentage | References |
|---|---|---|---|---|---|---|---|---|---|
| | SW Japan | | | 37 | 59 | | | 14 | |
| 1923 | Kanto (Tokyo), Japan | 7.9 | G, S | | 90 | 100 | 100 | | *Wald and Somerville* [1995] |
| 1944 | Tonankai, SW Japan | 8.1 | G,T, S | | 83 | 84 | 70 | | *Sagiya and Thatcher* [1999], *Tanioka and Satake* [2001b] |
| 1946 | Nankaido, SW Japan | 8.3 | G, T | | 55 | 84 | 70 | | *Sagiya and Thatcher* [1999], *Kikuchi and Yamanaka* [2001], *Tanioka and Satake* [2001a] |
| 1968 | Hyuga-nada, SW Japan | 7.5 | S | | 100 | 100 | 100 | | *Yagi et al.* [1998] |
| | Honshu | | | 65 | | | | 27 | |
| 1968 | Tokachi-Oki, Japan | 8.3 | T, S | | 100 | 100 | 81 | | *Satake* [1989], *Mori and Shimazaki* [1985] |
| 1994 | Sanriku, NE Japan | 7.7 | G, T, S | | 100 | 100 | 0 | | *Nakayama and Takeo* [1997], *Tanioka et al.* [1996] |
| | Hokkaido | | | 65 | | | | 27 | |
| 1952 | Tokachi-Oki, Japan | 8.4 | T | | 74 | 73 | 63 | | *Hirata et al.*, 2003 |
| | Kurile Island | | | 65 | | | | 27 | |
| 1958 | Etorofu, Kurile Islands | 8.3 | S | | 90 | 90 | 80 | | *Schwartz and Ruff* [1987] |
| 1963 | Etorofu, Kurile Islands | 8.5 | S | | 98 | 100 | 0 | | *Beck and Ruff* [1987] |
| 1969 | Shikotan, Kurile Islands | 8.2 | S | | 99 | 99 | 48 | | *Schwartz and Ruff* [1987] |
| 1973 | Nemoru-Oki, Kurile Islands | 7.8 | S | | 100 | 100 | 29 | | *Schwartz and Ruff* [1987] |
| | Kamchatka | | | | | | | | |
| 1952 | Kamchatka | 9.0 | T | 45 | 55 | 55 | 49 | 24 | *Johnson and Satake*, 1999 |
| | Alaska | | | | | | | | |
| 1938 | west of Kodiak | 8.3 | T, S | 29 | 75 | 100 | 100 | 21 | *Johnson and Satake* [1994], *Eastabrook et al.* [1994] |
| 1946 | Aleutians, Unimak Island | 8.3 | T | 41 | 58 | nd | nd | 46 | *Johnson and Satake* [1997] |
| 1957 | Aleutians, Andreanof Island | 8.6 | S, T | 52 | 76 | 76 | 50 | 14 | *Johnson et al.* [1994], *Boyd et al.* [1995] |
| 1964 | Prince William Sound | 9.2 | G, T, S | 26 | 33 | 52 | 43 | 17 | *Christensen and Beck* [1994], *Holdahl and Sauber* [1994], *Johnson et al.* [1996] |
| 1965 | Aleutians, Rat Island | 8.7 | S, T | 72 | 76 | 78 | 36 | 20 | *Beck and Christensen* [1991], *Johnson and Satake* [1996] |
| 1986 | Aleutians, Andreanof Island | 8.0 | S | 52 | 77 | 77 | 60 | 14 | *Houston and Engdahl* [1989], *Das and Kostrov* [1990] |
| 1996 | Aleutians, Delarof Island | 7.9 | S | 52 | 34 | 34 | 13 | 14 | *Schwartz* [1999], *Tanioka and Gonzalez* [1998] |
| | Mexico | | | | | | | | |
| 1981 | Michoacan | 7.3s | S | | | | | | *Mendoza* [1993] |
| 1985 | Michoacan | 8.1 | S | 29 | 59 | 72 | 65 | 20 | *Ruff and Miller* [1994], *Mendoza and Hartzell* [1989] |
| 1985 | Michoacan | 7.6s | S | | | | | | *Mendoza* [1993] |
| 1995 | Jalisco | 8.0 | S, G | 39 | 71 | 92 | 96 | 24 | *Zobin* [1997], *Azúa et al.* [2002] |
| | Peru | | | | | | | | |
| 1940 | Peru | 8.2 | S | 40 | 0 | 0 | 0 | 30 | *Beck and Ruff* [1987] |
| 1966 | northern Peru | 8.2 | S | 40 | 75 | 75 | 70 | 30 | *Beck and Ruff* [1987] |
| 1974 | Peru | 8.1 | S | 43 | 75 | 100 | 100 | 30 | *Hartzell and Langer* [1993], *Beck and Ruff* [1987] |
| 1996 | Peru | 8.0 | S | 23 | 30 | 60 | nd | nd | *Spence et al.* [1999] |
| | Chile | | | | | | | | |
| 1960 | south Chile | 9.5 | G | 35 | 67 | 96 | 88 | 29 | *Barrientos and Ward* [1990] |
| 1985 | Valparaiso | 8.0 | S, G | 41 | 83 | 63 | 17 | 10 | *Mendoza et al.* [1994], *Barrientos* [1988] |
| Average | 29 earthquakes | | | 42 | 71 | 79 | 57 | 23 | |
| % Total | all earthquakes | | | 41 | 55 | 69 | 46 | 21 | |
| % Total | Minus Alaska 64 | | | 52 | 68 | 73 | 47 | 24 | |
| % Total | Minus Alaska 64, Chile 60 | | | 56 | 69 | 72 | 45 | 15 | |

[a]G, T, and S are geodetic, tsunami, seismic waveform inversions, respectively. DSTL is deep-sea terrace free-air gravity low; asperity area is the measured area of highest slip contour or moment. Michoacan values are the sum of all three events. $M_s$ is surface wave magnitude; nd is not determined.

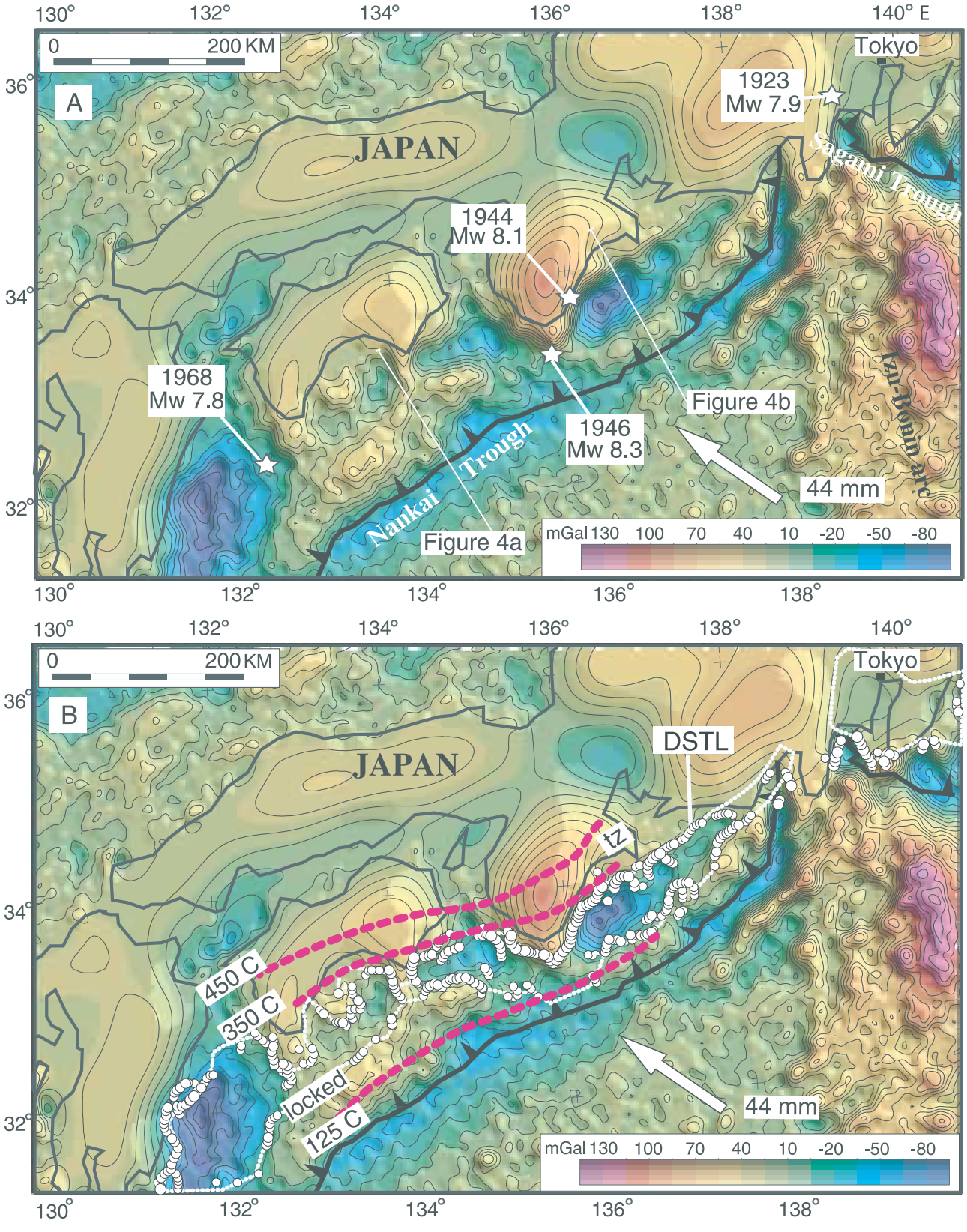


**Figure 3.** (a) Satellite free-air gravity map of Nankai convergent margin, SW Japan (this and all similar figures in this paper from data in the work of *Smith and Sandwell* [1997]). Epicenters of the largest twentieth century earthquakes located by stars (see Table 1). (b) DSTL defined by automated gradient picking (dotted line); circles show maximum gradients (many small gradients deleted for clarity). The 350°C isotherm on plate boundary fault [*Hyndman and Wang*, 1995b] coincides with gravity gradient along landward edge of basin-centered forearc lows (see basin locations in Figure 2). Convergence vectors in all the figures from *McCaffrey* [1993].

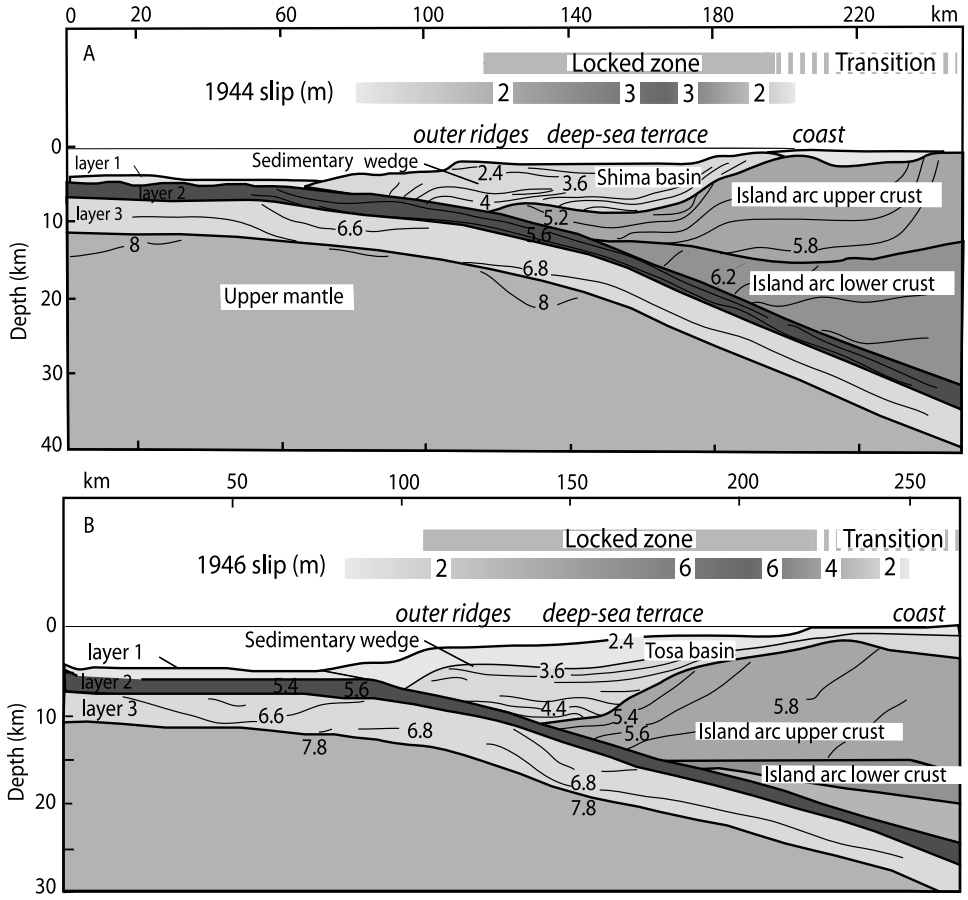


**Figure 4.** Seismic velocity structure of (a) 1944 Tonankai and (b) 1946 Nankai source regions, showing coseismic slip, and locked zone [*Nakanishi et al.*, 2002; *Kodaira et al.*, 2000; *Sagiya and Thatcher*, 1999; *Hyndman and Wang*, 1995a, 1995b]. Slip is focused beneath basins floored by thin wedge of arc crust. Profiles located in Figure 3.

that slip on splay faults is not required and that deep slip beneath the Muroto and Kii Peninsulas was largely aseismic. Coseismic slip determined from the 1944 seismic waveforms [*Kikuchi and Yamanaka*, 2001; *Kikuchi et al.*, 2003] also gives similar results (Figure 5a inset), indicating that slip was focused beneath the Shima and Kumano basins of segment C. Only deep slip occurred in segment D. The B–C boundary, which separates many of the historic earthquake pairs along the Nankai zone, is a pronounced gravity high with steep gradients that coincide with the 1944 and 1946 epicenters.

[11] For the Kanto earthquake of 1923, *Wald and Sommerville*'s [1995] combined inversion of geodetic, tsunami, and seismic waveforms outlines a well-constrained concentration of slip of up to 5 m beneath the Kanto basin southwest of Tokyo (Figure 5a). Ninety percent of the moment release occurred beneath the DSTL and 70% beneath the Kanto basin, but rapid sedimentation has filled the basin, and millions of people now live directly above the source zone. In the Tokai gap between the Tonankai and Kanto source zones, geodetic evidence indicates that a slip deficit beneath the Enshu and Senoumi basins D–E as in the work of *Sugiyama* [1994] is presently accumulating on the shallow megathrust, which last ruptured in 1854 [*Sagiya*, 1999; *Sagiya et al.*, 2000]. Finally, at the SW end of the Nankai trough, recent inversions of seismic waveforms from the 1968 Hyuga-nada earthquake [*Yagi et al.*, 1998] show that slip is focused beneath the northern end of the Hyuga basin and truncates against the transverse Ashizuri ridge separating it from the Tosa basin.

[12] For the great Nankai and Sagami trough events, about 60% of the total moment and more than 90% of the asperities by area (contoured area of highest slip value) occurred beneath the DSTL, and on average, 85% of the asperity areas occurred beneath the forearc basins (Table 1). The basins and source regions coincide with the thermally defined locked zone in the work of *Hyndman and Wang* [1995b]. The coincidence of the 350°C isotherm on the plate boundary with the sharply defined landward edge of the forearc basins revealed in the gravity data and the focus of high slip beneath each basin suggests a link between the earthquake process and basin geometry. The results are consistent with the segmented source models based on historic observations and confirm *Mogi*'s [1969] suggestion that great earthquake slip coincides with offshore topographic depressions.

### 3.2. Aleutian Islands

[13] The great 1957 central Aleutians and 1965 Rat Island events together ruptured nearly 1500 km of the plate

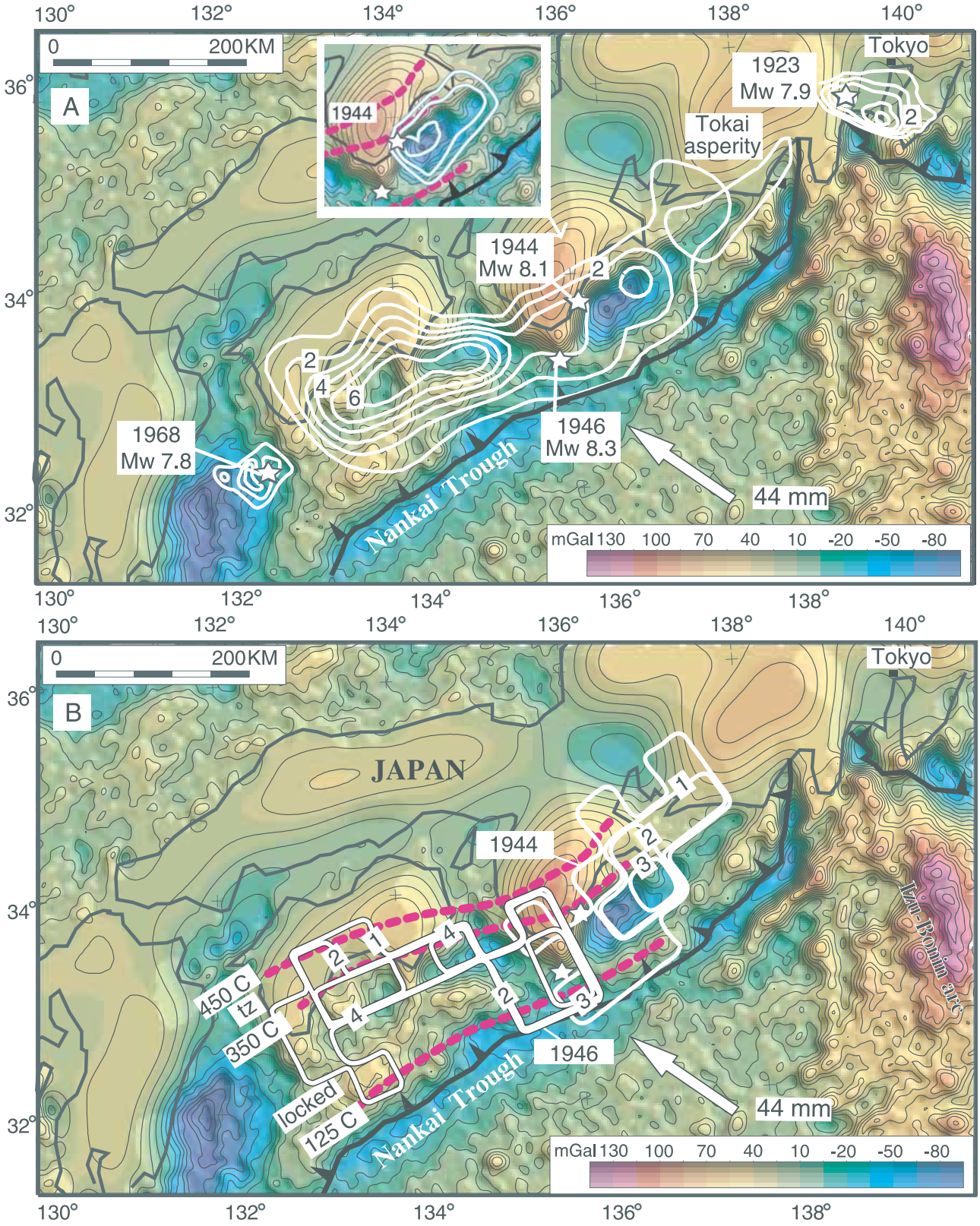


**Figure 5.** (a) Coseismic slip in meters (white contours) for 1923, 1944, 1946, and 1968 earthquakes on free-air gravity map, SW Japan; geodetic solution is for combined 1944 and 1946 events [*Wald and Somerville*, 1995; *Sagiya and Thatcher*, 1999; *Yagi et al.*, 1998]. Inset shows 1944 slip from strong-motion data alone [*Kikuchi and Yamanaka*, 2001] and generalized Tokai-locked asperity from GPS inversions [*Sagiya*, 1999; *Sagiya et al.*, 2000]. In general, high-slip is centered beneath basins, while epicenters (stars) tend to occur on gravity gradients. (b) Tsunami inversions for slip in the 1944 and 1946 earthquakes [*Tanioka and Satake*, 2001a, 2001b] are similar, with the greatest slip beneath the deep-sea terrace low, seaward of the 350°C isotherm.

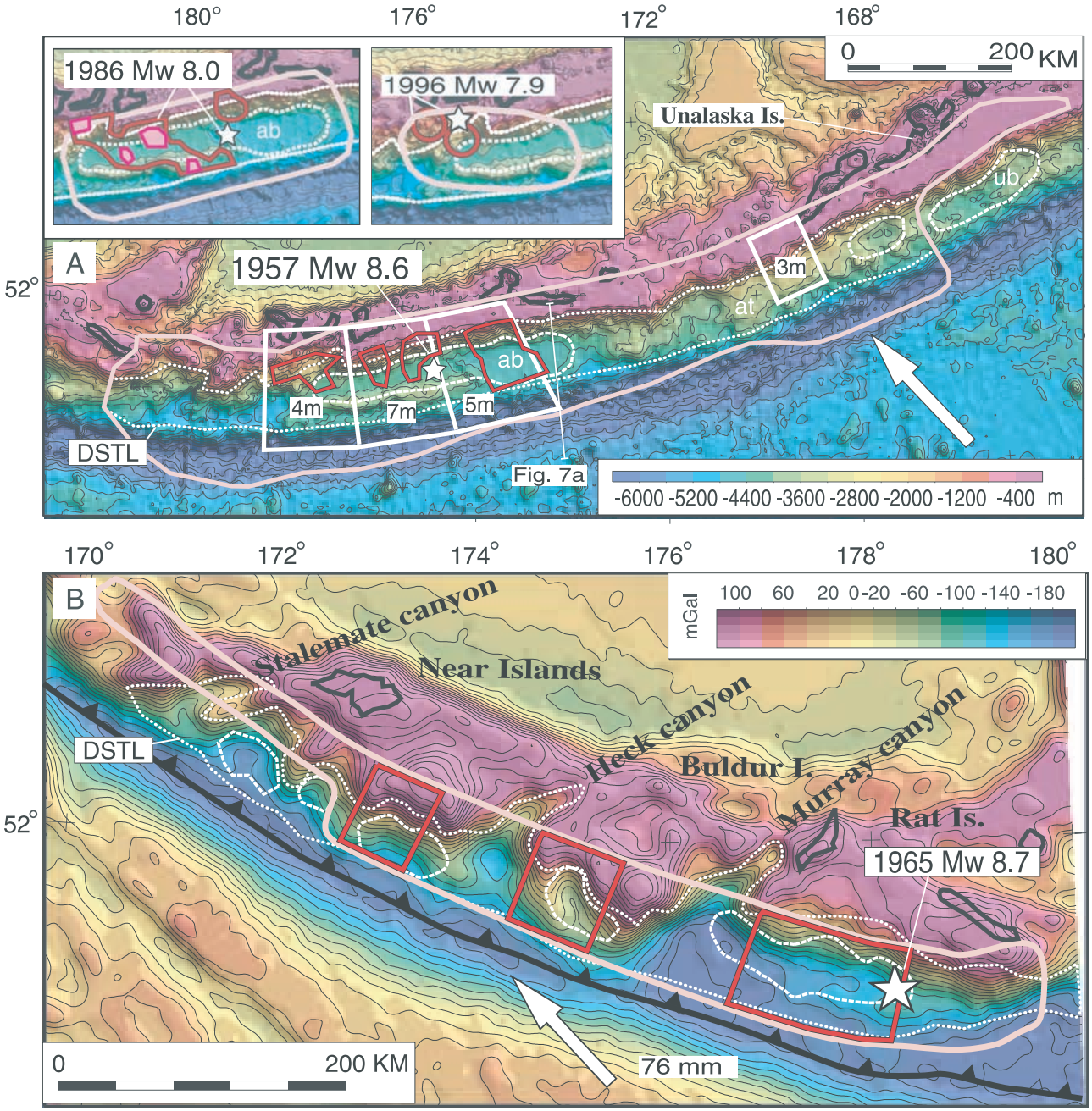


**Figure 6.** (a) Bathymetry and seismic slip, 1957 Aleutian Islands earthquake ($M_w$ 8.6). Epicenter (star), aftershock zone (pink line). Atka basin (ab) and Unalaska basin (ub) outlined by dashed white line; forearc bench at approximately 3500 m depth is Aleutian terrace (at); dotted line outlines DSTL. Subfaults (white boxes) with greatest coseismic slip in meters from tsunami inversion [*Johnson et al.*, 1994]. Red lines show maximum slip areas inferred from 1957 aftershock distribution [*Boyd et al.*, 1995]. Inset shows 1986 slip outlined by irregular red line, with greatest moment release in pink [*Das and Kostrov*, 1990]; the 1996 moment release in red circles [*Schwartz*, 1999]. Earthquakes ruptured Atka basin segment, most of the moment was released beneath DSTL, and asperities mostly filled gaps from earlier slip events [*Boyd et al.*, 1995; *Schwartz*, 1999]. (b) Bathymetry and seismic moment release, 1965 Rat Islands earthquake ($M_w$ 8.7); aftershock zone (pink) and areas of greater moment release (red) from *Beck and Christensen* [1991]. Moment appears to be released beneath forearc basin structures (dashed white lines) on leading edge of arc massif blocks.

boundary (Figures 6a and 6b). Slip was concentrated in five patches ranging from 50 to 300 km in length [*Johnson et al.*, 1994; *Beck and Christensen*, 1991; *Boyd et al.*, 1995]. For the 1957 earthquake ($M_w$ 8.6; Figure 6a), tsunami waveforms indicate that slip of up to 7 m was concentrated in a 275-km-long fault segment near the Andreanof Islands [*Johnson et al.*, 1994]. This very large asperity coincides with the largest forearc ridge and basin structure along the

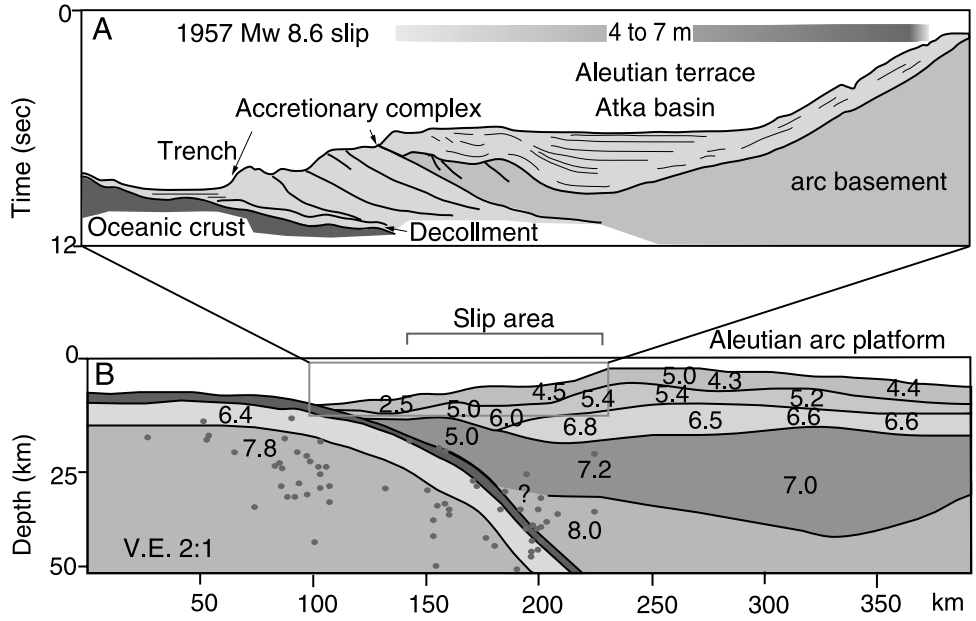


**Figure 7** Seismic reflection and velocity profiles across Aleutian arc [*Scholl et al.*, 1987; *Holbrock et al.*, 1999]. High-slip region during 1957 and 1986 earthquakes underlies Atka basin and Aleutian terrace, floored by a thin wedge of arc basement.

Aleutian terrace, the 380-km-long Hawley Ridge and Atka basin (Figures 6a and 6b) [*Scholl et al.*, 1987; *Ryan and Scholl*, 1993]. The Atka basin occupies a broad low on the terrace, which is inset into a very broad, concave embayment into the front of the Andreanof block. Seismic profiles across the slope terrace (Figures 7a and 7b) show that the basin is underlain by arc crust and is coincident with the source zone of the great earthquakes [*Scholl et al.*, 1987; *Ryan and Scholl*, 1993; *Holbrook et al.*, 1999]. Assuming that aftershocks in the epicentral region are anticorrelated with high-slip regions, *Boyd et al.* [1995] mapped potential asperities for the 1957 rupture that lie within the proposed source zone determined from the tsunami modeling (Figure 6a).

[14] The Atka basin source region ruptured again in the 1986 $M_w$ 8.0 Andreanof Islands and possibly in the 1996 $M_w$ 7.9 Delarof Islands earthquakes (Figure 6a inset) [*Houston and Engdahl*, 1989; *Das and Kostrov*, 1990; *Boyd et al.*, 1995; *Tanioka and Gonzalez*, 1998; *Schwartz*, 1999]. *Boyd et al.* [1995] showed that high-slip regions determined by *Das and Kostrov* [1990] for the 1986 event tend to fill the gaps between the high-slip regions they inferred for the 1957 rupture. Together, they nearly cover the entire Atka basin and the 1957 source zone calculated from tsunami data [*Johnson et al.*, 1994].

[15] East of the Atka basin, a much smaller patch of deep slip occurred in 1957, and no major slip occurred in any of the subsequent earthquakes. This part of the Aleutian terrace does not exhibit well-developed forearc basin morphology except for the 175-km-long Unalaska basin about 400 km to the east. Aftershocks in 1957 terminated eastward at the basin, which lies between the 1957 and 1946 ruptures (Figures 6a, 7a, and 8a). The 1957 aftershocks appear to wrap around the landward side of the Unalaska basin, possibly the location of a locked patch coincident with the "Unalaska Gap."

[16] For the 1965 Rat Islands earthquake ($M_w$ 8.7, Figure 6b), *Beck and Christensen* [1991] defined three areas of greater moment release that they correlated with strong blocks of arc crust forming the Rat, Buldur, and Near Islands blocks. *Geist et al.* [1988] interpreted these blocks to be rotating clockwise due to highly oblique subduction.

**Figure 8.** (opposite) (a) Coseismic slip and free-air gravity, 1938 ($M_w$ 8.2), 1946 earthquakes ($M_w$ 8.3), and Shumagin gap, sources in Table 1. Maximum slip from tsunami inversion (white subfaults with slip in meters) [*Johnson and Satake*, 1994] and maximum moment release from body and surface wave analysis (red circles proportional to moment) [*Eastabrook et al.*, 1994] occurred beneath Tugidak basin (tb) and Shumagin basin (sb) (dotted line). No slip or geodetic strain in Shumagin gap (shi) and low slip under Semidi Islands (si) transverse structural high [*Lisowski et al.*, 1988; *Freymueller and Beavan*, 1999]; red anticlines from *Plafker et al.* [1994]. Asperity for 1946 earthquake is not well defined (see text); ub, Unimak basin; wsab, west Sanak basin; sab, Sanak basin [*Bruns et al.*, 1987; *von Huene et al.*, 1987]. (b) Coseismic slip and free-air gravity, 1964 Prince William Sound earthquake ($M_w$ 9.2), slip from *Johnson et al.* [1996], see Table 1 for other sources. Relation of slip to DSTL is ambiguous; maximum slip occurs beneath gravity low of Prince William Sound (pws) and Dangerous Cape gravity high (dch) east of Kodiak Island. Intervening low-slip area coincides with transverse Portlock anticline (pa); dotted red magnetic anomaly marks present southern edge of Yakutat accreted terrane [*Plafker et al.*, 1994; *von Huene et al.*, 1999; *Brocher et al.*, 1994]; isotherms on plate boundary from *Oleskevich et al.* [1999].

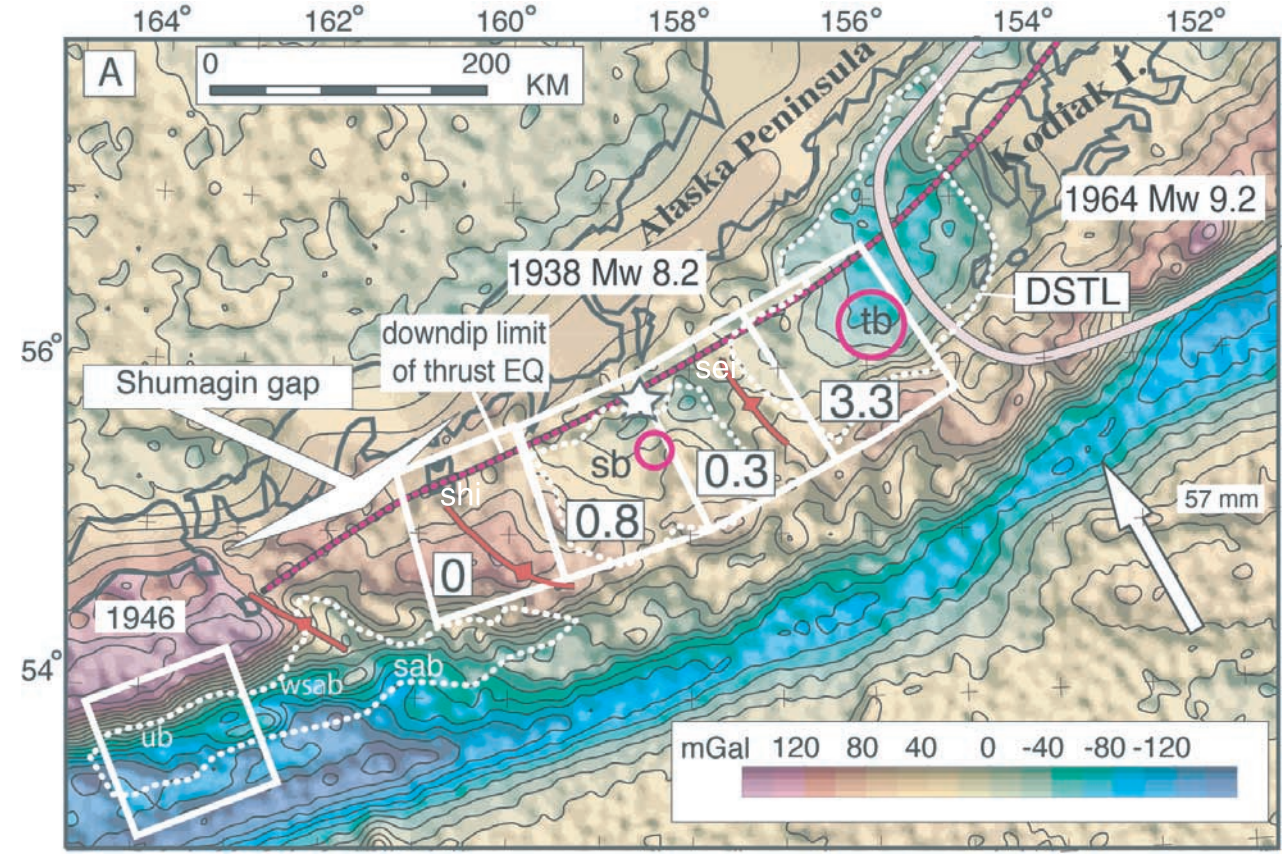
164°
162°
160°
158°
156°
154°
152°
A
0
200
KM
Alaska Peninsula
Kodiak I.
1964 Mw 9.2
1938 Mw 8.2
DSTL
tb
downdip limit
of thrust EQ
Shumagin gap
seg
3.3
sb
0.3
shi
0.8
0
57 mm
1946
wsab
sab
ub
56°
54°
mGal 120 80 40 0 -40 -80 -120

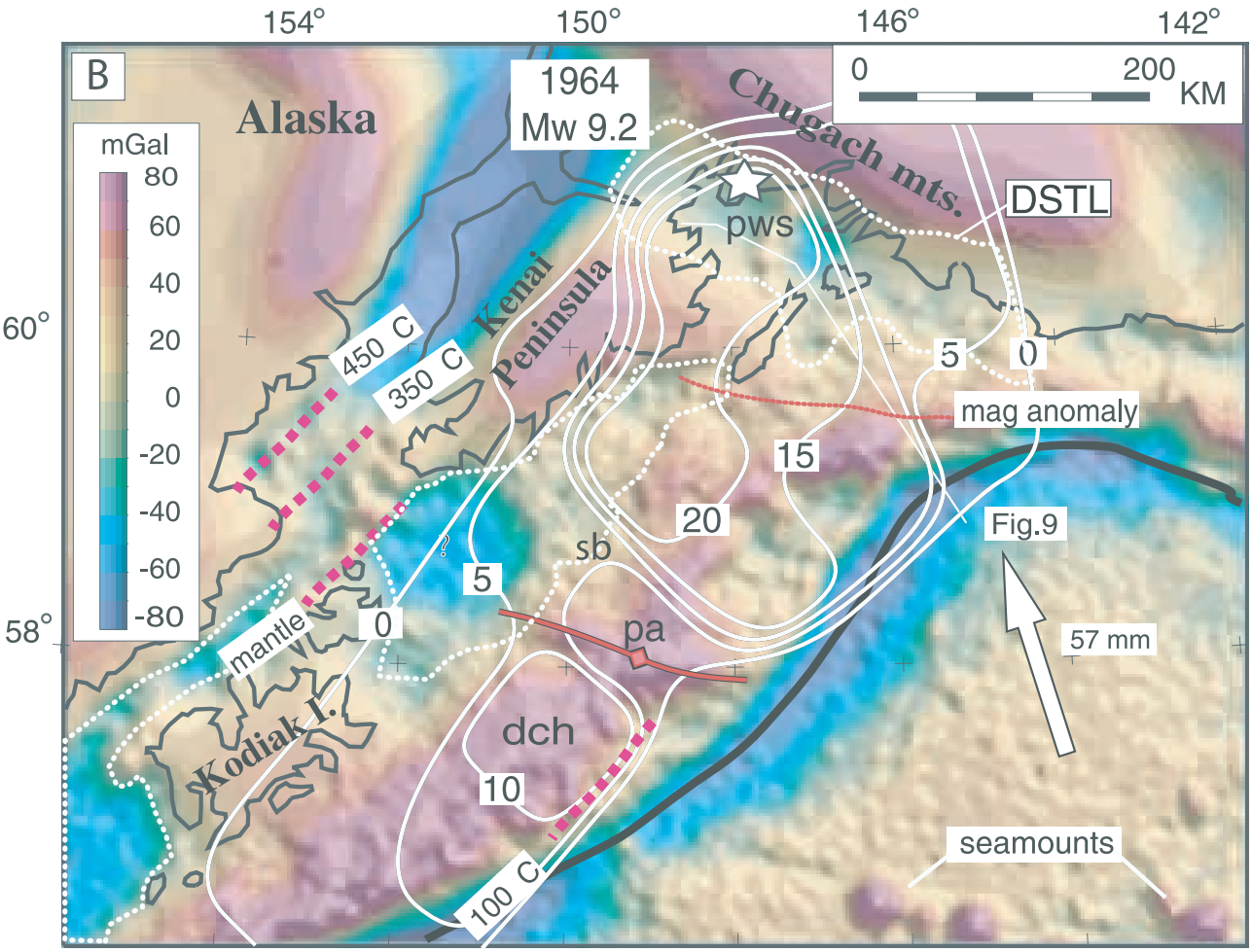
154°
150°
146°
142°
B
Alaska
1964
Mw 9.2
Chugach mts.
0
200
KM
mGal
80
60
40
20
0
-20
-40
-60
-80
DSTL
pws
Kenai
Peninsula
450 C
350 C
5
0
mag anomaly
15
20
Fig.9
sb
5
pa
mantle
0
57 mm
Kodiak I.
dch
10
seamounts
100 C
60°
58°

Most of the 1965 aftershocks were concentrated along the highly sheared and presumably weaker transverse block boundary faults following the canyons between the blocks [*Beck and Christensen*, 1991; *Ryan and Scholl*, 1993]. Transverse canyons cut the Aleutian terrace along the Rat Islands rupture, and the leading edges of the blocks form a series of concave embayments in the slope terrace. On the basis of the bathymetry and seismic reflection profiles similar to those across the Atka basin to the east [*Vallier et al.*, 1994], the leading edges of each block are interpreted as a series of forearc basins on a discontinuous slope terrace. The asperities of *Beck and Christensen* [1991] tend to coincide with the location and size of the slope basins. The tsunami inversion of *Johnson and Satake* [1996] shows three similar source regions along strike, but using the 18°-dip of the focal plane as the source, they inferred significant slip deep beneath most of the arc platform. However, more recent estimates of the depth of the megathrust beneath the central part of the Aleutian platform suggest that it is deeper than 75 km, presumably below the limit of seismic slip (Figure 7b, see also http://neic.usgs.gov/neis/bulletin/03_EVENTS/eq_030317 for a recent seismicity cross section through the Rat Islands). It is not clear what the effect of changing the fault geometry would have on the slip distribution determined from tsunami waveforms.

[17] For the 1957, 1965, and 1986 events, more than 75% of the area of the seismically defined asperities lie beneath the DSTL, and about half of the highest slip area lies beneath the forearc basins, which cover less than 20% of the rupture area.

### 3.3. Southern Alaska

[18] The broad continental shelf of southern Alaska is underlain by a sequence of filled Cenozoic forearc basins developed on a basement of Mesozoic to modern accretionary complexes that become younger toward the trench [*Plafker et al.*, 1994]. The subducting Pacific plate is nearly flat lying beneath the margin, and subduction is complicated by the collision and subduction of the Cretaceous and early Tertiary oceanic Yakutat terrane beneath SE Alaska and Prince William Sound. The structure of the sediment-filled Cenozoic basins is outlined by abundant seismic data [e.g., *Bruns et al.*, 1987; *von Huene et al.*, 1987; *Fisher et al.*, 1987; *Plafker*, 1987], and the basin structures are recognizable as basin-centered lows in the satellite gravity data (Figures 8a and 8b). Most of the southern Alaskan subduction zone, with the conspicuous exception of the Shumagin gap, ruptured in the great 1938, 1946, and 1964 earthquakes.

[19] For the $M_w$ 8.2 earthquake of 1938 (Figure 8a), inversion of tsunami waveforms indicates that slip of 3.3 and 0.8 m was focused at the eastern and western ends of the rupture, respectively [*Johnson and Satake*, 1994]. Little or no slip occurred in the Shumagin gap or in the central part of the rupture. Slip was concentrated in the segments containing the Tugidak and Shumagin forearc basins, whereas little or no slip occurred beneath transverse structural highs of the Shumagin Islands and the Semidi Islands. These structures separate the basins and may be inherited structures, now reactivated by migration of the forearc (axes of uplift in red in Figure 7a) [*von Huene et al.*, 1987; *Bruns et al.*, 1987]. Seventy-five percent of the seismic moment as determined from the tsunami inversion was released beneath the DSTL, and 100% of the asperities defined by seismic means [*Eastabrook et al.*, 1994] occurred beneath the basins (Table 1).

[20] The 1946 $M_w$ 8.3 earthquake west of the Shumagin gap (Figure 8a) occurred beneath the Unimak basin [*Bruns et al.*, 1987], but the wave height of the resulting tsunami was much larger than expected for the magnitude of the earthquake [*Johnson and Satake*, 1997] and the source is problematic. *Fryer and Watts* [2001] argued that the tsunami source involved submarine sliding, and *Plafker et al.* [2001] measured wave heights of up to 40 m on Unimak Island consistent with massive submarine landsliding during the earthquake. The resolution of the source model is not sufficient to interpret the relation between seismic slip and structure.

[21] Sustained post middle Miocene to Holocene subsidence is recorded by the fill in the Tugidak, Shumagin, Sanak, and Unimak basins [*von Huene et al.*, 1987; *Bruns et al.*, 1987], and *Bruns et al.* [1987] argued that subduction erosion is the likely cause for subsidence of the Sanak and Unimak basins. The actively subsiding forearc basins are coincident with areas of slip in 1938 and 1946 and suggest a link between seismic slip and basin formation. The transverse highs may represent future asperities that have not yet slipped or alternatively may be poorly coupled to the downgoing plate. No strain is presently accumulating in the Shumagin gap [*Lisowski et al.*, 1988; *Freymueller and Beavan*, 1999], suggesting that weak coupling beneath the Shumagin transverse high is more likely. By contrast, the Tugidak basin appears on the basis of recent GPS inversions to be the locus of a contemporary locked patch [*Zweck et al.*, 2002].

[22] Slip during the 1964 Prince William Sound earthquake ($M_w$ 9.2) shows an ambiguous relationship to forearc gravity lows (Figure 8b). The major asperity coincides with the present-day subduction of the mafic Yakutat terrane into the seismogenic zone [*Plafker et al.*, 1994; *Brocher et al.*, 1994; *Christensen and Beck*, 1994; *Holdahl and Sauber*, 1994; *Johnson et al.*, 1996]. The region of greatest slip (>20 m) in Prince William Sound largely follows a local gravity low and avoids the Kenai Peninsula high, but high slip continues offshore beneath another gravity high underlain by the accreted Prince William terrane. A second asperity off Kodiak is centered on the Dangerous Cape high, an area of late Cenozoic uplift and beveling [*von Huene et al.*, 1987], also probably underlain by accreted oceanic Prince William terrane. The region of low slip between Kodiak and the main asperity coincides with the transverse Portlock anticline. Like the Shumagin Islands, this low-slip area may reflect low strain accumulation associated with a transverse uplift. Presently, this area is accumulating strain more slowly than the Prince William and Tugidak asperities [*Zweck et al.*, 2002]. The lack of correlation between forearc lows and slip in the great Alaska earthquake is in large part due to the anomalous outer arc gravity high. The high may be caused by the unusually flat-lying, dense lower plate, a local doubling of oceanic crustal thickness, and resultant uplift of the upper plate due to the collision of the Yakutat terrane (Figure 9) [*Brocher et al.*, 1994].

### 3.4. Southern Chile

[23] Along the southern Chile margin, slip inversions are available for two earthquakes, the great 1960 $M_w$ 9.5

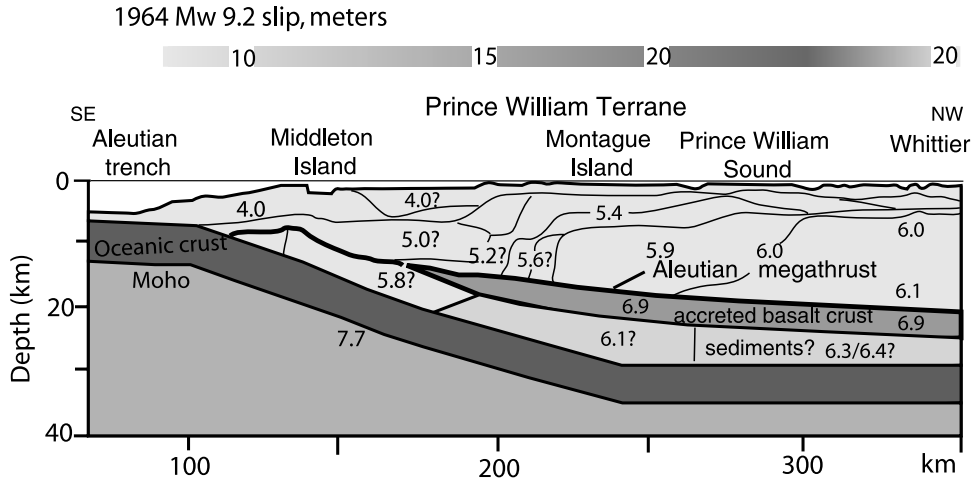


**Figure 9.** Seismic velocity profile across the Prince William Sound asperity of the 1964 great Alaska earthquake [*Brocher et al.*, 1994]. Location shown in Figure 8. Subducting plate is nearly flat and is thickened by subduction of Yakutat terrane.

southern Chile event and the 1985 $M_w$ 8.0 Valparaiso earthquake (Figure 10). In the Valparaiso area, the 1985 event was preceded by the 1906 ($M_s$ 8.3), 1943 ($M_w$ 7.8), and 1971 ($M_w$ 7.8) earthquakes [*Tichelaar and Ruff*, 1991; *Compte et al.*, 1986; *Mendoza et al.*, 1994]. The Valparaiso sequence occurred in a broad embayment in the margin extending from 30° to 36°S that coincides with a large offshore gravity low (Figure 10a). The low marks a series of filled slope basins resting on thinned continental crust that extends to within 50 km of the trench (Figure 11) [*Flueh et al.*, 1998; *von Huene et al.*, 1997]. *Laursen et al.* [2002] have interpreted the largest of these basins, the Valparaiso basin (Figure 11a), to be the result of subsidence from enhanced basal erosion during subduction of seamounts of the Juan Fernandez Ridge.

[24] The source region for the 1971 earthquake appears to lie largely beneath the Valparaiso slope basin, but unfortunately, there are no slip inversions available for this earthquake. For the 1985 Valparaiso earthquake, inversion of strong-motion, teleseismic, and long-period Rayleigh waves [*Mendoza et al.*, 1994] shows that slip occurred largely offshore and updip of the hypocenter, between 55 and 10 km depth. The slip maxima occurred beneath the shelf edge at Valparaiso and offshore beneath the terrace (Figure 10a); a smaller asperity occurred beneath the Valparaiso basin, where large slip presumably occurred in 1971. No slip data are available for the 1943 and 1906 events, but together with 1971 and 1985, they appear to fill the proposed source region for a 1730 event coincident with the broad embayment marked by the DSTL [*Compte et al.*, 1986]. South of the embayment, the conception gravity high separates the Valparaiso embayment from the northern limit of the great 1960 rupture.

[25] In the source region of the 1960 Chile earthquake, the world's largest instrumentally recorded event ($M_w$ 9.5 or 9.6) [*Cifuentes*, 1989; *Barrientos and Ward*, 1990], the margin structure is similar to Valparaiso. The trench is filled with sediment, but only a modest accretionary prism has formed, and continental crust extends to within 30 km of the trench, suggesting subsidence and subduction erosion of the forearc [*Plafker*, 1972; *Bangs and Cande*, 1997]. For the 1960 earthquake (Figure 10b), there is a coincidence between the size and distribution of the forearc basins and the distribution of coseismic slip determined from geodetic data and relative sea level change [*Barrientos and Ward*, 1990]. Although the offshore basins are filled with sediment and have little bathymetric expression, they have been mapped with seismic reflection surveys (Figure 11b) [*Mordojovich*, 1981] and are visible as a chain of pronounced lows in the satellite gravity data.

[26] The high-slip region of *Barrientos and Ward* [1990] follows the axis of six basin-centered gravity lows, and most of the lows coincide with local slip maxima, with slip in excess of 30 m occurring beneath the largest basins. The geodetic slip distribution underestimates the total moment determined from seismic methods and could be biased by the lack of tsunami data [*Barrientos and Ward*, 1990]. Given those caveats, 67% of the shallow, geodetically determined coseismic moment occurred beneath the DSTL, and nearly 90% of the asperities by area occurred beneath the offshore sedimentary basins. The inboard edge of the basins is marked by a steep gravity gradient coincident with the landward decrease in fault slip. This is similar to SW Japan, although the projected 350°C isotherm [*Oleskevich et al.*, 1999] lies inboard of the slip gradient and the basin margins. The slip patches are roughly bounded by the subducted fracture zones on the downgoing plate, suggesting that the margin is seismically segmented [*Barrientos and Ward*, 1990]. The basins also seem to be bounded by the incoming fracture zones and tend to be centered over the coherent crustal blocks rather than the transverse boundaries.

## 4. Earthquakes at Nonaccretionary Margins

### 4.1. Hokkaido, Kurile Islands, and Kamchatka

[27] Between 1952 and 1994, a series of seven earthquakes $\geq M_w$ 7.7 ruptured much of the plate boundary off northern Honshu, Hokkaido, the Kurile Islands, and Kamchatka (Table 1 and Figure 12). This margin is sediment starved, and the offshore forearc consists of a broad deep-sea terrace with little or no active accretionary wedge. Off

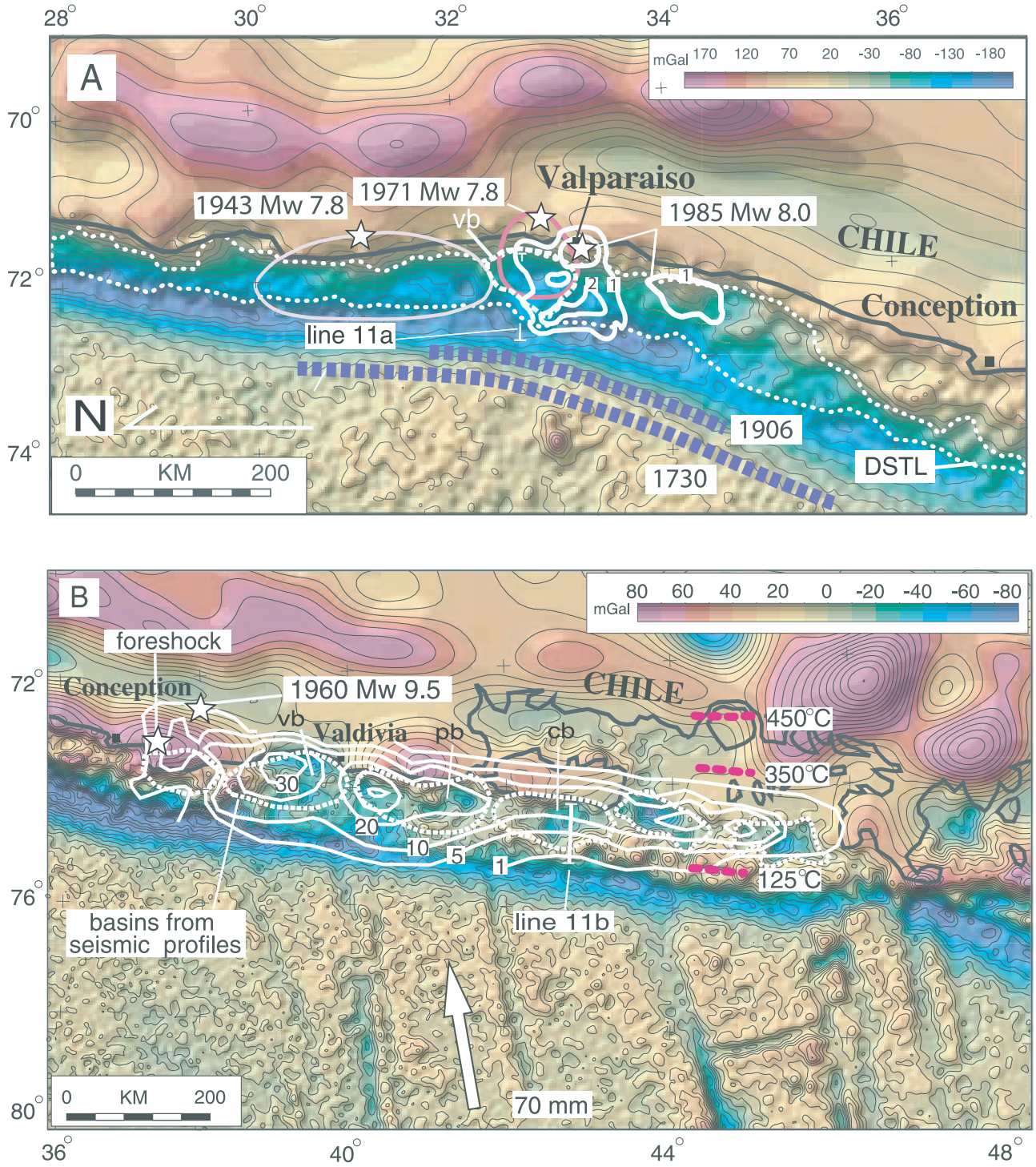


**Figure 10.** (a) Coseismic slip and free-air gravity, 1985 $M_w$ 8.1 Valparaiso, Chile earthquake. Slip in meters (white contours) on megathrust underlies coastal gravity gradient and offshore DSTL; vb is Valparaiso basin. Slip distribution from *Mendoza et al.* [1994]. (b) Coseismic slip and free-air gravity, 1960 $M_w$ 9.6 Chile earthquake. Greatest coseismic slip correlates with gravity lows centered on late Cenozoic basins, including those at Valdivia, Pucatrihue, and Chiloe (vb, pb, cb, dashed lines), identified in seismic profiles. Slip distribution as in the work of *Barrientos and Ward* [1990], with deep aseismic slip deleted for clarity; thermal model from *Oleskevich et al.* [1999].

Honshu, the terrace is underlain by Mesozoic arc crust with crustal velocities [*Finn et al.*, 1994; *Tsuru et al.*, 2000] and is veneered by a thin cover of Cenozoic sediment [*von Huene et al.*, 1994] (Figure 13). Well-developed forearc basins like those off Nankai are not apparent, but local depressions in the terrace off Hokkaido are observed in the gravity data, especially on either side of Cape Erimo, where seamounts are being subducted (Figure 12).

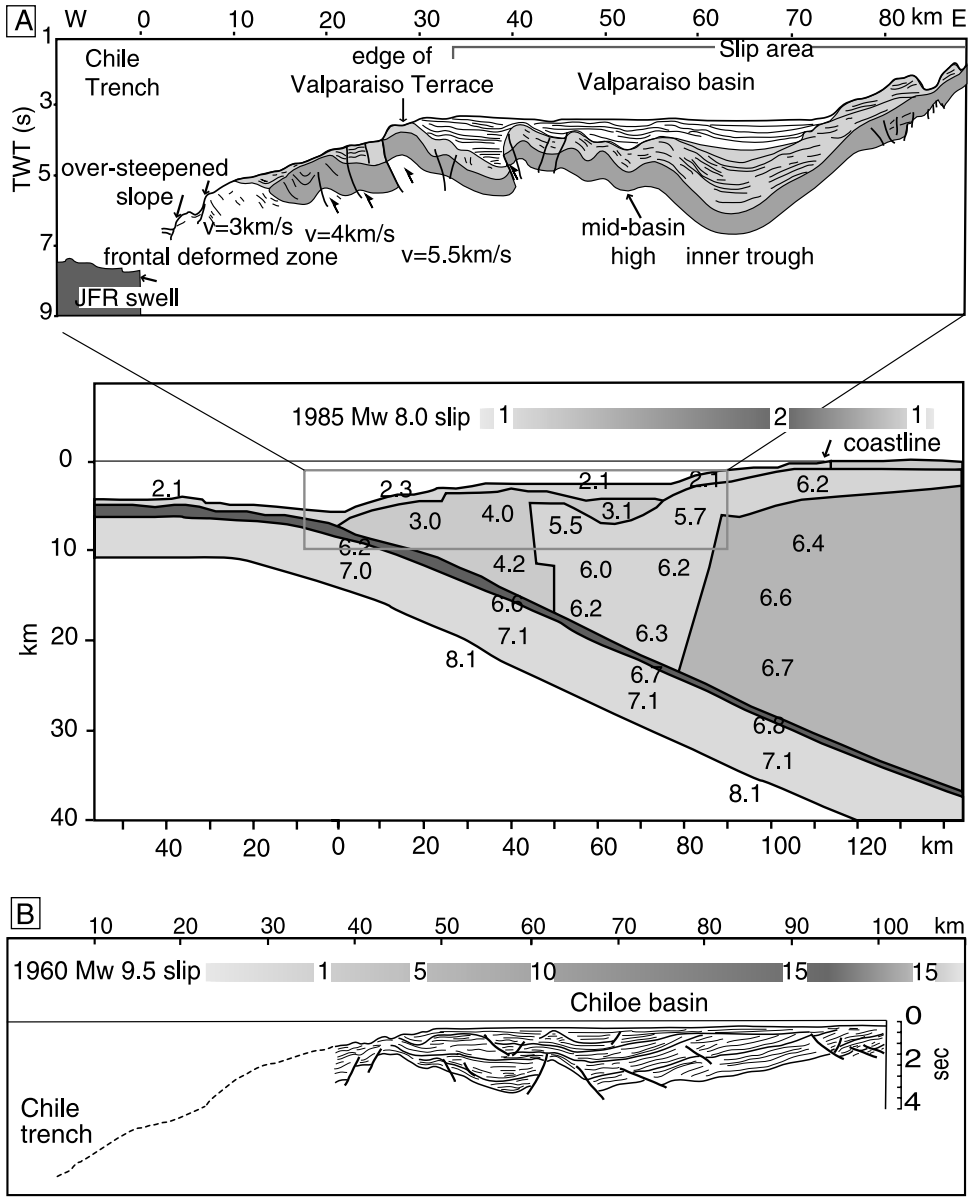


**Figure 11.** (a) Seismic reflection and velocity profiles across Valparaiso basin and source region of 1985 Valparaiso earthquake ($M_w$ 8.0) [*Laursen et al.*, 2002; *Flueh et al.*, 1998]. Slip occurs beneath area of sustained subsidence interpreted to be the result of basal subduction erosion. (b) Seismic reflection profile across outer shelf and slope off Chile Island [*Mordojovich*, 1981], source region of great 1960 Chile earthquake ($M_w$ 9.6). Basin is underlain by continental crust, which extends nearly to the trench. High coseismic slip occurs beneath the basin.

[28] Slip in the 1994 $M_w$ 7.7 Sanriku-Oki earthquake was determined from tsunami waveforms by *Tanioka et al.* [1996] and from strong-motion data by *Nakayama and Takeo* [1997]. During the Sanriku-Oki earthquake, more than 1 m of slip occurred in several asperities across the width of the slope terrace. Coseismic slip was determined for the 1952 ($M_w$ 8.4) and 1968 ($M_w$ 8.3) Tokachi-Oki events from inversion of tsunami waveforms [*Hirata et al.*, 2003; *Satake*, 1989], and for the 1968 event, from inversion of seismic waves [*Schwartz and Ruff*, 1985; *Mori and Shimazaki*, 1985; *Kikuchi and Fukao*, 1985]. For the 1968 event, the slip distributions are generally similar [*Satake*, 1989], and the results of *Satake* [1989] are shown in Figure 12a. Slip of up to 4 m in 1968 was concentrated under the prominent embayment south of Cape Erimo. The 1952 $M_w$ 8.4 Tokachi-Oki earthquake occurred in the embayment off Hokkaido and had two high-slip regions (Figure 12). Deep slip in excess of 5 m occurred beneath a well-defined gravity low on the slope terrace, and shallow slip in excess of 7 m occurred beneath the outer slope [*Hirata et al.*, 2003]. Source regions for the earthquakes off the Kurile Islands, 1958 $M_w$ 8.3, 1963 $M_w$ 8.5, 1969 $M_w$ 8.2, and 1973 $M_w$ 7.8, were determined from seismic waveforms by *Schwartz and Ruff* [1985, 1987] and *Beck and Ruff* [1987]. In all these events, the epicenters occur beneath the bathymetric and gravity gradient marking the landward

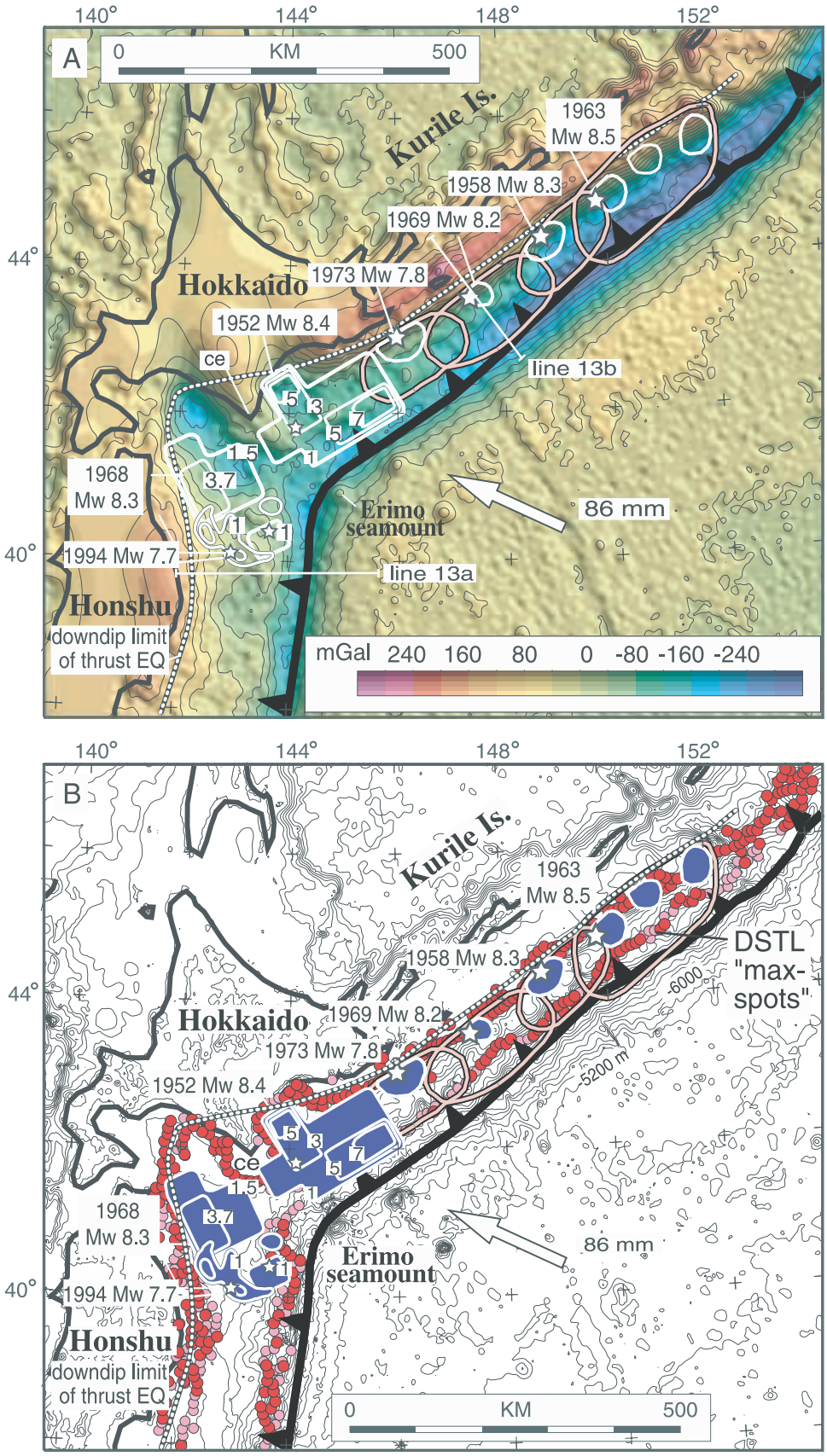
A
B
140°
144°
148°
152°
44°
40°
0
KM
500
Kurile Is.
Hokkaido
Honshu
1963
Mw 8.5
1958 Mw 8.3
1969 Mw 8.2
1973 Mw 7.8
1952 Mw 8.4
1968
Mw 8.3
1994 Mw 7.7
ce
5
3
7
5
1
1.5
3.7
1
1
line 13b
line 13a
Erimo
seamount
86 mm
downdip limit
of thrust EQ
mGal 240 160 80 0 -80 -160 -240
DSTL
"max-
spots"
-6000
-5200 m

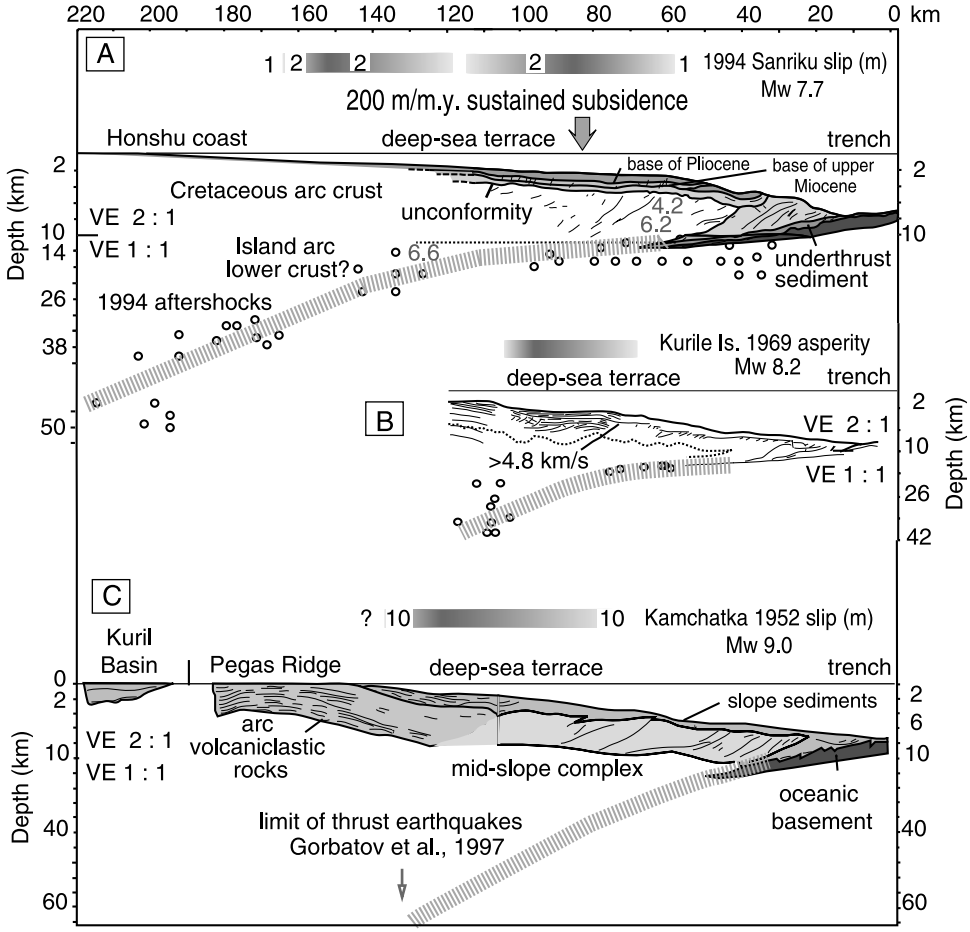


**Figure 13.** (a) Seismic profile near the source region of 1994 Sanriku-Oki earthquake ($M_w$ 7.7) [*von Huene et al.*, 1994; *Tsuru et al.*, 2000]. Vertical exaggeration is 2:1 above 10 km depth, 1:1 below for all profiles. Aftershocks, fault, and high-slip regions [*Nakayama and Takeo*, 1997] projected 40 km along strike onto profile. Deep-sea terrace and thinned arc crust above source region have undergone sustained late Cenozoic subsidence due to basal subduction erosion. (b) Seismic profile through source region of 1969 Shikotan earthquake, Kurile Islands [*Klaeschen et al.*, 1994]. Normal faulted arc massif overlain by erosional unconformity and slope sediments, suggesting significant subsidence above high moment release area from *Schwartz and Ruff* [1987]. (c) Seismic profile through source zone of great 1952 Kamchatka earthquake ($M_w$ 9.0; see Figure 14) [*Klaeschen et al.*, 1994; *Gorbatov et al.*, 1997]. Deep-sea terrace coincides with zone of high slip at depth 10–12 m [*Johnson and Satake*, 1999], which we infer extends to about 60 km depth, the downdip limit of thrusting [*Gorbatov et al.*, 1997].

edge of the slope terrace, and the maximum moment release occurs beneath the slope terrace or the upper slope (Figures 12 and 13).

[29] Although the resolution of the source inversions vary along strike, the high-slip areas match the width of the slope terrace, which narrows from 100 km off Honshu to less than 30 km off the northern Kurile Islands. The downdip limit of thrust focal mechanisms [*Tichelaar and Ruff*, 1993] and the downdip limit of slip in the great earthquakes closely follow the gravity gradient along the inboard edge of the slope terrace (Figure 12b). The high-slip regions in 1952 and 1968 both avoid the prominent structural high at Cape Erimo. The slope terrace appears to be a geomorphic proxy for the areas of maximum moment release that underlie it;

**Figure 12.** (opposite) (a) Coseismic slip, seismic moment release, and aftershock zones on free-air gravity for 1952, 1958, 1963, 1968, 1969, 1973, and 1994 earthquakes, Honshu, Hokkaido, and Kurile Islands. Stars mark epicenters; white contours show coseismic slip in meters on subfaults from tsunami modeling of 1952 and 1968 fault source regions [*Hirata et al.*, 2003; *Satake*, 1989] and seismic inversion of 1994 Sanriku-Oki earthquake [*Nakayama and Takeo*, 1997]. For Kurile earthquakes, solid white lines show maximum moment release with aftershock zones in pink [*Schwartz and Ruff*, 1987; *Beck and Ruff*, 1987]; dotted black and white line is landward limit of thrust focal mechanisms [*Tichelaar and Ruff*, 1993]. (b) High-slip regions (blue) lie almost entirely within DSTL outlined by gravity gradient (red circles). Slip avoids Cape Erimo (ce) high.

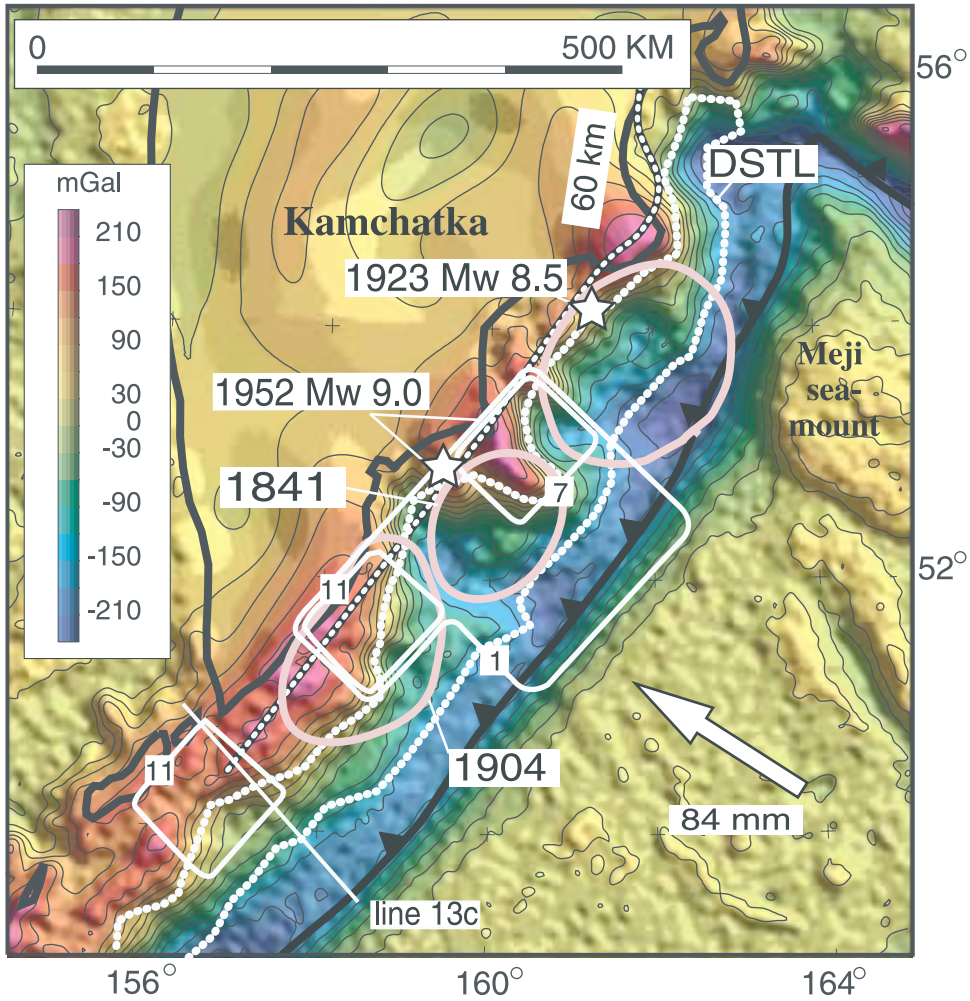


**Figure 14.** The 1952 great earthquake ($M_w$ 9.0) and free-air gravity, Kamchatka. Coseismic slip in meters on subfaults from tsunami waveform inversion (white contours), modified from *Johnson and Satake* [1999]. Epicenters and source zones are shown for prior great earthquakes (stars; pink lines). See text for discussion.

nearly 95% of the seismic moment and asperities in this earthquake sequence occurred beneath the DSTL.

[30] Off Honshu, the deep-sea terrace records sustained subsidence over Neogene time (Figure 13a). The sedimentary cover on the terrace rests on a subaerial unconformity dated at about 20 Ma, which now lies between 2 and 4 km depth [*von Huene and Scholl*, 1991; *von Huene et al.*, 1994]. *von Huene and Scholl* [1991] argued that this subsidence can only be achieved through basal subduction erosion of the forearc by the downgoing plate. The coincidence between the source regions of the great earthquakes and the subsiding terrace is consistent with *Mogi*'s [1969] observation and suggests that subduction erosion and seismic slip may be related.

[31] Off Kamchatka, the margin is marked by major embayments and slope basins (Figure 14), some of which may have been created by erosion during subduction of large seamounts, like the Meji seamount, now entering the trench [*Geist and Scholl*, 1994]. Although the scalloped slope break is highly irregular, its landward edge generally coincides with the 60-km-deep downdip limit of thrust focal mechanisms [*Gorbatov et al.*, 1997] and the epicenters of great earthquakes [*Johnson and Satake*, 1999]. For the 1952 Kamchatka event ($M_w$ 9.0), *Johnson and Satake* [1999] identified three asperities with 6–12 m of slip from tsunami modeling (Figure 14). Two asperities coincide with slope terrace reentrants that we suggest are related to subsidence interpreted from seismic profiles (Figures 13b and 13c) [*Klaeschen et al.*, 1994], but the resolution is not sufficient to address the relation in detail. We infer that modeled slip landward of the 60-km-limit of thrust focal mechanisms may be an artifact of the constant 13°-dip of the subfaults in the tsunami model. Only modest slip was centered beneath the major basins in 1952, whereas 7 m of slip was centered on a prominent transverse gravity high. No tendency toward slip beneath the major forearc basins is evident, although great earthquakes did occur beneath the coastal embayments in 1923 and possibly in 1841 [*Johnson and Satake*, 1999].

### 4.2. Mexico and Peru

[32] In northern Mexico (Figure 15a), seismic slip for the 1985 great Michoacan earthquake sequence ($M_w$ 8.1) and for the 1981 earthquake in the same area has been determined by *Mendoza and Hartzell* [1989] and *Mendoza*

[1993]. *Ruff and Miller* [1994] also determined areas of maximum moment release for most of the earthquakes. Slip for the 1981 event, main shock, and large aftershock ($M_s$ 7.6) is combined in Figure 15a, and it occurs mostly beneath the slope terrace low within a broad coastal embayment. The highest slip in the main shock (5–6.5 m) occurred along the landward edge of the rupture near the coast, and significant slip apparently occurred up to 50 km inboard of the coast at the western end of the rupture. In the 1995 Jalisco earthquake ($M_w$ 8.0), slip determined from seismic waveform modeling [*Zobin*, 1997] was shallow and largely occurred beneath two slope depressions separated by a bathymetric high. Inversions of GPS campaign measurements put the highest slip (>3 m) beneath the westernmost of the two marginal lows [*Azúa et al.*, 2002]. Seismic profiles off northern Mexico [*Khutorskoy et al.*, 1994] are not optimally oriented to address offshore basin geometry but do show that the Manzanillo basin overlies the seismically determined high-slip area at the east end of the rupture. A similar gravity low coincides with the high-slip region in the western part of the rupture. Deep submersible investigations off Manzanillo reveal continental plutons overlain by an erosional unconformity on the lower slope, implying sustained subsidence and subduction erosion [*Lepinay et al.*, 1997]. However, the basin origin is complicated by its relationship to the offshore projection of the Colima graben [*Khutorskoy et al.*, 1994]. Between 60 and 70% of the seismic moment in this earthquake sequence occurred beneath the DSTL, and 80% of the mapped area of asperities occurred beneath offshore structural depressions inferred from the gravity.

[33] Off Peru, a series of great earthquakes between 1940 and 1974 ruptured much of the Nazca-South America plate boundary between the subducting Nazca Ridge and the Mendana fracture zone (Figure 15b). This sequence may represent rerupturing of the source region of the great 1746 earthquake [*Beck and Ruff*, 1987], which coincides with a broad embayment in the margin containing the 500-km-long Lima slope basin. The entire slope is underlain by crystalline continental crust, and little or no accretion occurs at the trench [*von Huene and Scholl* [1991]. Sustained subsidence of the slope at 500 m/m.y. over the past 5 Ma are recorded by a subaerial unconformity beneath the basin, which is overlain by shallow water late Miocene benthic foraminifera now at more than 3 km depth [*von Huene and Lallemand*, 1990]. Figure 16 illustrates a composite section of the central Peru source region in which we have projected the 1974 rupture surface 100 km along the strike of the trench onto the seismic reflection interpretation in the work of *von Huene and Lallemand* [1990]. The section indicates that subsidence of the Lima basin is coincident with areas of maximum slip and moment release determined for the 1966 ($M_w$ 8.2) and 1974 ($M_w$ 8.1) earthquakes [*Beck and Ruff*, 1987*;Hartzell and Langer*, 1993]. Five of the seven major asperities in the 1940–1966–1974 great earthquake sequence lie beneath the Lima basin, and a sixth lies beneath the lower slope. The 1940 and 1970 epicenters lie landward of the others, suggesting that deeper slip may also occur. For the 1996 event ($M_w$ 8.0), which occurred where the Nazca Ridge is subducting, the moment distributions are inconsistent. *Spence et al.* [1999] modeled slip that extended to an unusually deep 66 km, whereas *Swenson and Beck* [1999] place the major moment release at about the same distance from the hypocenter but near the coastline at shallower depths. *Spence et al.* [1999] resolved the slip onto the preferred focal plane (33° dip), so shallow slip is poorly resolved.

## 5. Discussion

### 5.1. Characteristics of the Earthquake Source Zones

[34] The observed relationship of coseismic slip to subduction zone structure is schematically summarized in Figure 17. The source areas are largely offshore beneath the slope and outer shelf, consistent with the observations of *Tichelaar and Ruff* [1993] and *Ruff and Tichelaar* [1996], who suggested that the downdip limit of large seismic slip correlates in a general way with the coastline. Most of the seismic slip occurs beneath the deep-sea terrace and its basins. This part of the forearc is characterized by a prominent DSTL, which comprises on average, about 41% of the seismogenic zone by area. The landward edge of the DSTL forms a strong gradient near the shelf-slope break (see Figures 3 and 12). Within the DSTL lie the mapped forearc basins, which occupy about 21% of the seismogenic zone by area. About 71% of an earthquake's seismic moment, on average, is released beneath the DSTL (Figures 5–17 and Table 1). For the asperities, 79% of an earthquake's area of highest contoured slip value or moment underlies the DSTL, on average, and 57% underlies the forearc basins. If we sum the moment from all the earthquakes, about 55% occurs beneath the DSTL, but our results are skewed by the 1964 Alaska earthquake ($M_w$ 9.2), whose forearc gravity signature has been much modified by the present-day collision of the Yakutat block (see earlier discussion). If we exclude this earthquake, 68% of the remaining seismic moment is released beneath the DSTL, a value which remains stable even if we also exclude the 1960 Chile event ($M_w$ 9.6).

[35] Seismic slip decreases landward across the strong gravity gradient marking the landward edge of the forearc basins and the DSTL. In the northwest Pacific, the computer-picked gradients outlining the DSTL are an excellent predictor of the limits to large seismic slip (Figure 12b). This appears to be the case in general, although there are exceptions in Mexico, Peru, and Chile, where large seismic slip locally occurs landward of the DSTL (Figure 14). The limit of slip is presumably controlled by the depth to the mantle or by the thermal transition to stable sliding [e.g., *Hyndman and Wang*, 1995a, 1995b; *Oleskevich et al.*, 1999]. Along the Nankai margin, for example, the lower boundary of coseismic slip in excess of 1 m coincides approximately with the 450°C isotherm, and the largest slip, in excess of 4–6 m, is bounded by the 350°C isotherm along the back edge of the DSTL (Figure 5). In some great earthquakes, the tsunami inversions indicate that the updip limit of slip appears to be close to the trench [*Johnson et al.*, 1996; *Tanioka and Satake*, 2001a, 2001b; *Hirata et al.*, 2003]. In general, however, the highest slip region tends to be deeper beneath the forearc basins and the upper slope.

[36] Can we conclude from these observations that the asperities tend to occur beneath the DSTL and its sedimentary basins? To answer this question, we set up the following null hypothesis: Although the asperities have finite areal extent, together they occupy only a small proportion (11%) of the seismogenic zone. Thus we treated the position of the

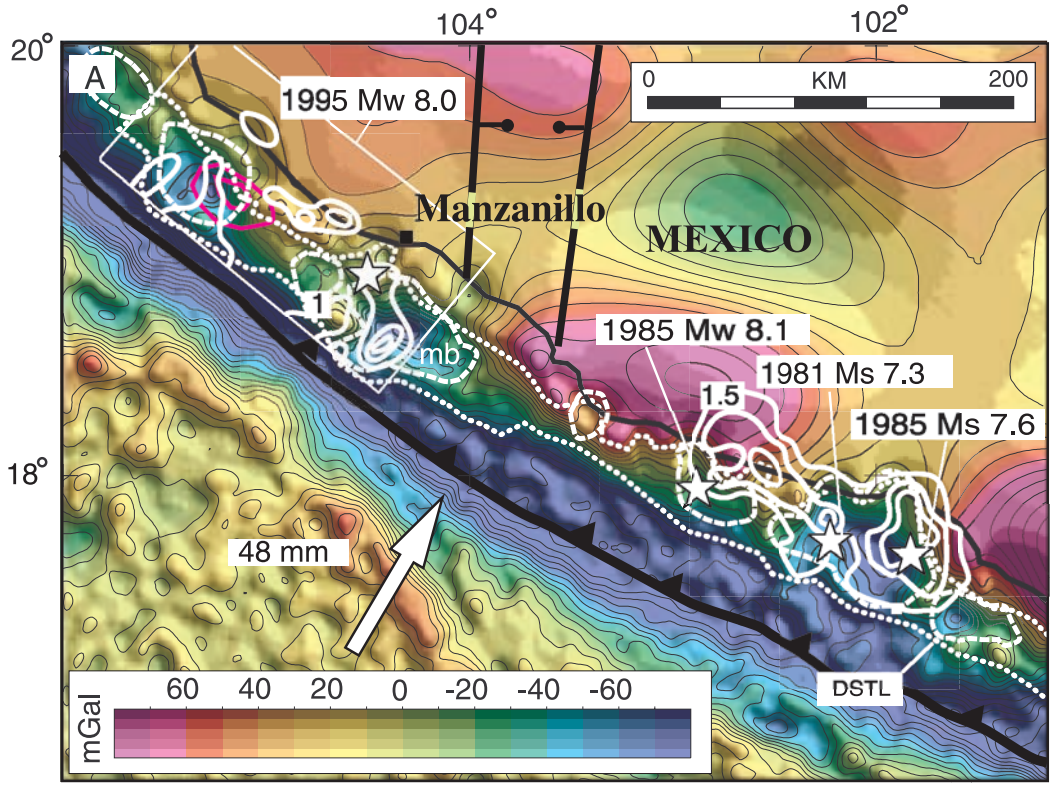
104°
102°
20°
18°
A
1995 Mw 8.0
0
KM
200
Manzanillo
MEXICO
1
mb
1985 Mw 8.1
1981 Ms 7.3
1.5
1985 Ms 7.6
48 mm
mGal
60 40 20 0 -20 -40 -60
DSTL

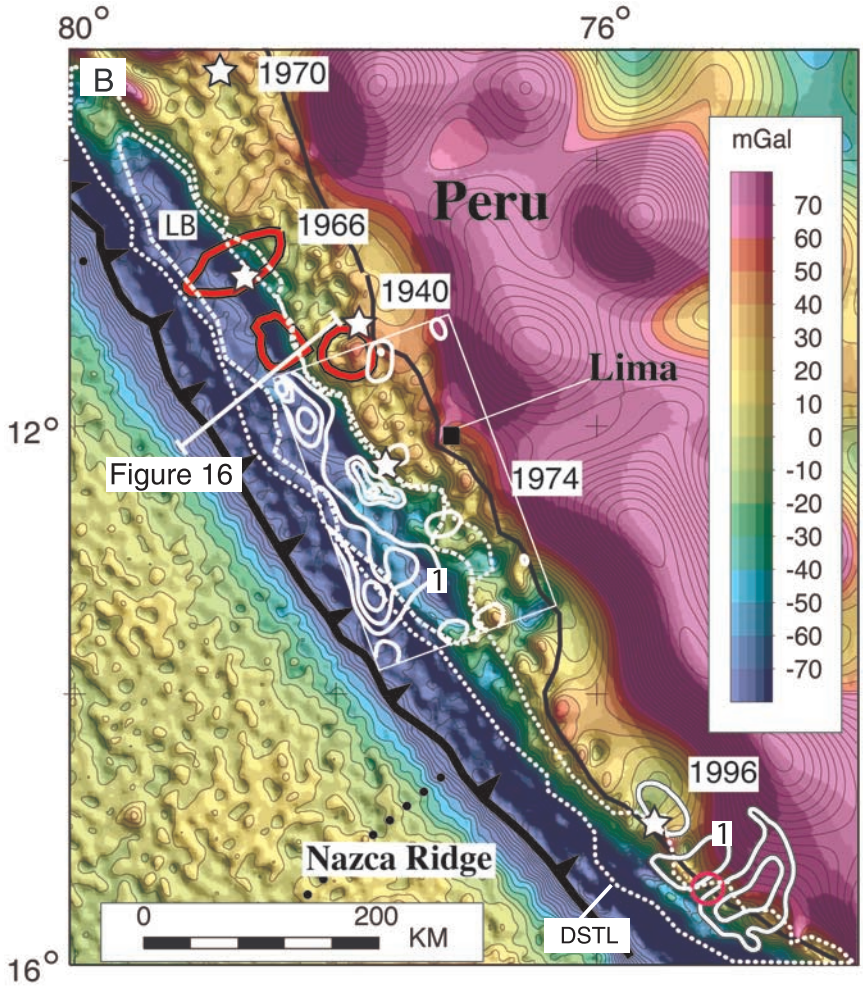
80°
76°
12°
16°
B
1970
LB
1966
Peru
1940
Lima
Figure 16
1974
1
mGal
70
60
50
40
30
20
10
0
-10
-20
-30
-40
-50
-60
-70
1996
1
Nazca Ridge
0
200
KM
DSTL

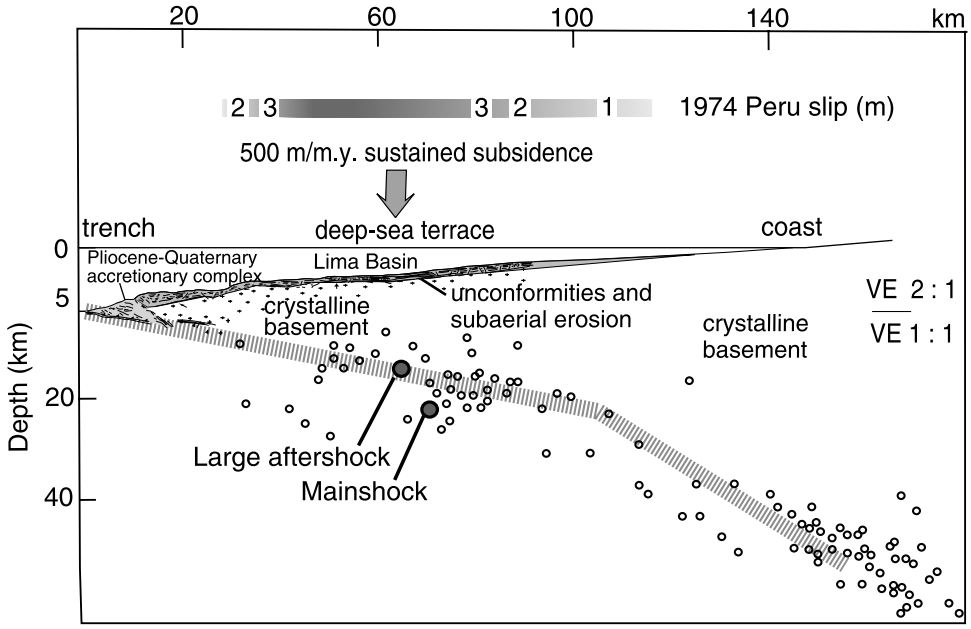


**Figure 16.** Composite cross section of Peru margin. Slip surface of 1974 earthquake projected along strike of margin onto line drawing of seismic profile of Peru margin and Lima basin [*Hartzell and Langer*, 1993; *von Huene et al.*, 1988; *von Huene and Lallemand*, 1990]. High-slip region in this margin segment underlies thinned continental crust and basin, which has undergone sustained late Cenozoic subsidence. Thinning and subsidence are interpreted to be the result of basal subduction erosion along the plate boundary [*von Huene and Lallemand*, 1990], apparently coincident with source region.

center of each asperity (53 asperities in 29 earthquakes) as an independent random event, falling either inside or outside the mapped projection of sedimentary basins. This constitutes a binomial process with well-known probability distributions. If individual events are randomly located, the probability of falling beneath a sedimentary basin is equal to the ratio of the area occupied by all sedimentary basins and the area of the seismogenic zone, namely 0.21. Given this probability for individual events, the probability that 27 out of 53 random points will fall beneath sedimentary basins is vanishingly small. We repeated the experiment for the 43 asperities that fell within the DSTL with even more dramatic results. Thus we reject the null hypothesis that asperities are randomly located and conclude that the asperities in our sample of great earthquakes tend to fall beneath the DSTL and its basins.

[37] Although any one inversion could be biased by its assumptions and uncertainties, we are encouraged by the overall correlation of slip with geologic structure. The commonly observed trenchward decrease in seismic slip could reflect some landward bias in the geodetic observations, but the tsunami and seismic inversions give similar results and suggest that the pattern of deeper, basin-centered asperities is real. Some of the trenchward propagating coseismic slip may be accommodated by out-of-sequence thrusting on splay faults [e.g., *Plafker*, 1972; *Sagiya and Thatcher*, 1999; *Park et al.*, 2002]. The permanent shortening rate in the accretionary prism may approximate the convergence rate [e.g., *von Huene and Klaeschen*, 1999], but it is unclear when the shortening occurs in the seismic cycle. Although the prism is relatively aseismic [*Byrne et al.*, 1988], a few of the tsunami inversions document some coseismic slip beneath the prism. Our statistics suggest, however, that low-slip areas outside the DSTL are more likely to be areas that undergo significant aseismic slip during the seismic cycle, rather than potential future asperities.

### 5.2. Along-Strike Variability in Coseismic Slip

[38] Along strike, the deep-sea terrace and its basins are commonly segmented by fault zones and uplifts that are transverse to the convergent margin. These intrabasin structures are generated by along-strike changes in plate geom-

**Figure 15.** (opposite) (a) Seismic slip and free-air gravity, 1985 $M_w$ 8.1 Michoacan and 1995 $M_w$ 8.0 Jalisco earthquakes, northern Mexico. Michoacan slip is combined from 1985 main shock, major 1985 aftershock, and 1981 earthquake [*Mendoza and Hartzell*, 1989; *Mendoza*, 1993]. Symbols as above. Onshore faults outline Colima graben. Jalisco slip from seismic inversion as in the work of *Zobin* [1997] and 3- and 5-m contours (red) of GPS inversion [*Azúa et al.*, 2002]. Most of the slip underlies slope depressions (dashed line, from gravity data; mb is Manzanillo basin). (b) Seismic slip (white contours, in meters), high moment release (red), and free-air gravity, 1940, 1966, 1970, 1974, and 1996 Peru earthquakes. Slip in 1974 [*Hartzell and Langer*, 1993] mostly underlies subsiding Lima basin (lb, dashed white line) and lower slope, as do aftershock regions of 1966 event. Slip during 1996 ($M_w$ 8.0) Nazca Ridge earthquake extended to 66 km [*Spence et al.*, 1999], but shallow slip is poorly resolved. High moment release as in the work of *Swenson and Beck* [1999], indicated by red circle.

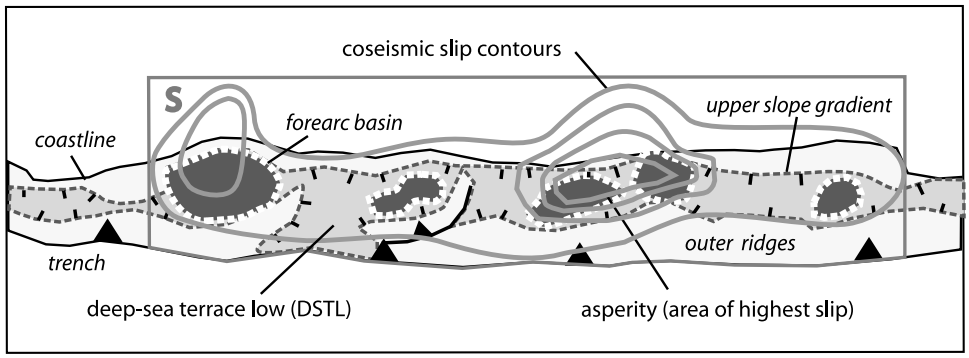


**Figure 17.** Subduction zone cartoon summarizing observations of 29 of the largest Circum-Pacific megathrust earthquakes. S is seismogenic zone, with downdip limit of coseismic slip from thrust focal mechanisms, thermal or geodetic models, or mantle depth. The DSTL comprises on average 41% of S but contains 71% of an earthquake's seismic moment and 79% of its asperity area (area of highest slip). Mapped forearc basins comprise 21% S and contain 57% of an earthquake's asperity area, on average.

etry and strain partitioning in the upper plate. Common causes of structural segmentation of the overlying plate include incoming fracture zones [e.g., *Barrientos and Ward*, 1990; *Ryan and Scholl*, 1993], oblique subduction and margin parallel deformation [e.g., *Sugiyama*, 1994; *Geist et al.*, 1988], inherited transverse structures [*Bruns et al.*, 1987], and ridge subduction and seamount "tunneling" [e.g., *von Huene et al.*, 1997; *Laursen et al.*, 2002].

[39] Several of the transverse, intrabasin highs in our study apparently overlie areas of lower slip in great earthquakes. The 1952 and 1968 great earthquakes off Hokkaido ruptured on either side of the gravity high at Cape Erimo (Figure 12), but little or no slip occurred beneath the Cape in either earthquake. Thus the Cape is either a potential asperity storing up great slip to be released in a future earthquake, or it is relatively weak, possibly because of trapped heat or fluids beneath the thicker crust. Inversion of the contemporary GPS velocity field at Cape Erimo is consistent with less than full locking of the underlying plate boundary [*Mazzotti et al.*, 2000]. A weaker fault beneath the Cape could allow some aseismic slip there, causing earthquakes to nucleate along the Cape Erimo gradient and rupture primarily under the adjacent basins. A similar pattern occurred in the 1944 Nankai event, which nucleated on the margin of the Kii Peninsula uplift, but largely ruptured beneath the adjacent basin (Figure 5). Off Alaska, the Shumagin Islands high or Shumagin "gap" (Figure 8), exhibited no coseismic slip in 1938 or 1946, and it is presently accumulating little elastic strain, indicating poor coupling with the downgoing plate [*Lisowski et al.*, 1988; *Freymueller and Beavan*, 1999]. We wonder if margin-normal anticlinal highs might also be more resistant to bending during elastic loading of the upper plate and thus generate less slip during earthquakes. The combination of a weak fault and an upper plate locally resistant to compression might explain the low coseismic slip at Cape Erimo in 1952 and 1968, Shumagin Islands and Semidi Islands in 1938, and the Portlock anticline in 1964.

[40] Not all forearc highs, however, are areas of lower seismic slip. In the 1952 Kamchatka earthquake, one of the three asperities was centered on a prominent transverse high separating two large basins (Figure 14), and in the 1946 Nankaido event, significant slip occurred beneath the southwestern Kii Peninsula (Figure 5). Along the Nankai margin, the transverse anticlinal highs accommodate significant oblique slip on splay faults and may be important components of coseismic deformation. Splay faults were explicitly included in the geodetic inversion of *Sagiya and Thatcher* [1999] for slip in 1944 and 1946 but were not required in the tsunami inversions of *Tanioka and Satake* [2001a, 2001b].

[41] The tendency for coseismic slip to be focused beneath the terrace and its basins, rather than beneath the intervening highs, could reflect along-strike variations in the temperature, fluid pressures, and stresses on the megathrust caused by variations in overlying crustal thickness and density. Large-scale segmentation of the source zone would then result from oblique convergence, subducting fracture zones, or some other second-order process. The subbasin megathrust segments may simply represent what is left of an ideally more continuous seismogenic zone. However, the question remains whether there is a relationship between forearc basin evolution and seismogenesis.

### 5.3. Sustained Subsidence Above the Seismic Source Zone: A Link to Subduction Erosion?

[42] Megathrust source zones tend to remain beneath sea level in the absence of major accretionary events, even though the upper plate is commonly uplifted many meters in each great earthquake. In contrast, coastal ranges landward of the source often exhibit long-term uplift and shortening, even though they commonly coincide with the axis of subsidence during great earthquakes [e.g., *Plafker*, 1972]. The long-term pattern reflects the interseismic deformation and suggests that some interseismic strain is permanent and not recovered during earthquakes [e.g., *Kelsey et al.*, 1994; *von Huene and Klaeschen*, 1999]. Although long-term subsidence offshore could result from sediment loading or cooling of the forearc [*Dickinson*, 1995], we suggest that permanent interseismic subsidence may also contribute to formation of the deep-sea terrace above the source zone.

[43] The deep-sea terrace and its basins are commonly underlain by a seaward thinning wedge of relatively high-velocity continental or arc crust (Figures 4, 13, and 16) [e.g., *Holbrook et al.*, 1999; *Parsons et al.*, 1998; *Kodaira et al.*, 2000; *Nakanishi et al.*, 2002]. The characteristic

deep-sea terrace profile (e.g., Figures 4, 7, and 11) is thought to reflect increasing strength of the arc basement beneath the terrace [*Byrne et al.*, 1988]. However, off Peru, Mexico, Alaska, and NE Japan, the crustal wedge is overlain by late Cenozoic shallow-water sediments now at depths of 2–4 km. Sustained subsidence, confirmed by ocean drilling program (ODP) and seismic profiling, is characteristic of these slope terraces. *Von Huene and Scholl* [1991] have argued that such large subsidence must be caused by basal erosion of the forearc by the downgoing plate. Basal erosion rates of 25–50 km$^3$/m.y. per km of trench length are indicated for Peru, NE Japan, and northern Chile, and erosion is documented off Costa Rica, Ecuador, Alaska, and many other margins [*Scholl et al.*, 1980; *von Huene and Lallemand*, 1990; *von Huene and Scholl*, 1991; *Ranero and von Huene*, 2000; *Collot et al.*, 2002; *Scholl et al.*, 2002]. Enhanced erosion has occurred along some margins where seamounts and aseismic ridges are being subducted, for example, at Valparaiso, Chile; Kamchatka, and Alaska [*Laursen et al.*, 2002; *Bruns et al.*, 1987]. Along accretionary margins, higher rates of sediment accretion make it more difficult to quantify the role, if any, of basal subduction erosion in the development of the forearc. Basal erosion could be occurring there as well, given that the sediment flux into subduction zones commonly exceeds the rate of growth of forearc accretionary prisms [*von Huene and Scholl*, 1991; *Scholl and von Huene*, 2001].

[44] Where data on sustained subsidence are available, the inferred locus of subduction erosion appears coincident with the source zone of great earthquakes (compare Figures 13 and 16). Perhaps this correlation is fortuitous, with erosion resulting from unrelated ridge and seamount subduction. However, circumstantial evidence for subduction erosion exists for seven of the margins we examined (see earlier descriptions), suggesting that it may be common along convergent margins. Although it is difficult to document widespread erosion without more deep seismic reflection and drilling, we find the apparent correlation between subduction erosion and great earthquakes intriguing, as it may provide a mechanism to explain our observation that seismic slip tends to occur beneath sedimentary basins.

[45] If subsidence, subduction erosion, and seismogenesis are coincident in many of our subduction zones, we can consider the possibility that tectonic erosion is occurring during earthquakes. The erosion rate would then be proportional to the seismic slip rate and the basin subsidence rate. Typical long-term subsidence rates of the slope are 0.2–0.5 km/m.y. and subduction erosion rates are 25–50 km$^3$/m.y. per km of margin [*von Huene and Scholl*, 1991]. The subsidence rates from erosion are similar to the average sedimentation rate of forearc basins in general (0.1–0.3 km/m.y. [*Dickinson*, 1995]). If the rate of erosion was distributed over an average seismogenic width of about 100 km with a convergence rate of 50 mm/yr, the channel delivering material to depth would be 0.5–1.0 km thick. Assuming rupture over the entire seismogenic width and a 100-year recurrence interval, average subduction erosion during a great earthquake would remove the equivalent of 2–5 cm from the upper plate over the rupture surface. The amount removed from the upper plate could represent part of the interseismic strain not recovered during the earthquake.

[46] The process by which basal subduction erosion might occur, either by grain-by-grain plucking or fault propagation into the upper plate, is uncertain. *Ranero and von Huene* [2000] interpreted "mega-lenses" 10–15 km wide and 1–2 km thick on seismic reflection profiles across the Costa Rica and Nicaraguan plate boundary as fault-bounded slices eroded off the base of the forearc. This process is apparently occurring in the seismogenic zone. At the downdip termination of seismic slip, it is unclear what happens to the eroded material. Some sediment may be transferred back to the upper plate landward of the coastline to produce the commonly observed long-term uplift of the coastal ranges in forearcs. Basal subduction erosion of the forearc might eventually flatten the seaward taper of the forearc and weaken it, possibly leading to margin-normal shortening to reestablish a critical taper [*Willett*, 1992]. This may happen in some accretionary margins [*McNeill et al.*, 2000], but it does not appear to be occurring in nonaccretionary margins, which are commonly characterized by gently seaward-dipping mid-Cenozoic strata resting on arc or continental basement (Figures 13 and 16).

### 5.4. Basin-Centered Gravity Lows as Proxies for Long-Term Coseismic Slip: Implications for Cascadia

[47] The empirical relationship between seismic slip and forearc gravity and bathymetric lows suggests that the geometry of the DSTL and its forearc basins may be a proxy for the long-term coseismic slip distribution along some subduction zones. The Cascadia subduction zone in the northwestern United States and adjacent Canada was the source of an $M_w \sim 9$ earthquake and tsunami in 1700 A.D. [*Atwater and Hemphill-Haley*, 1997; *Satake et al.*, 1996]. From the tsunami wave heights in Japan, average fault slip of about 15 m has been estimated for the offshore source region [*Satake and Wang*, 2000, also written communication, 2002]. The inboard edge of Cascadia's offshore, basin-centered gravity lows may indicate the likely inboard limit of major slip for great earthquakes, where no seismicity or historical data are available to constrain the downdip limit of slip.

[48] The shelf and slope appear on isostatic residual gravity maps to be organized into a series of lows which coincide with the major late Cenozoic basins recognized in seismic profiles (Figures 18 and 19) [*Snavely*, 1987; *Clarke*, 1992; *Parsons et al.*, 1998; *McNeill et al.*, 2000]. The basin-centered lows overlie the megathrust source region inferred from geodetic and thermal models [*Hyndman and Wang*, 1995a; *Oleskevich et al.*, 1999]. The basins overlie a thin wedge of high-velocity forearc crust (Figure 19), and the Newport basin appears to record a 30-million-year history of subsidence above the subduction zone [*Snavely et al.*, 1980]. Active upper plate folds and faults analogous to the Cape Muroto-type structures of SW Japan separate the basins and accommodate margin parallel shortening [*McNeill et al.*, 1998]. Broadly speaking, the gravity lows can be divided into five major segments separated by transverse uplifts at Port Alberni, Quinault, Heceta Head, and Cape Blanco. The lows are similar to the offshore basins along the Nankai trough (Figures 2 and 3) and suggest that the Cascadia subduction zone is segmented into large rupture patches that correlate with offshore gravity lows. The largest is 300 km long, off Washington

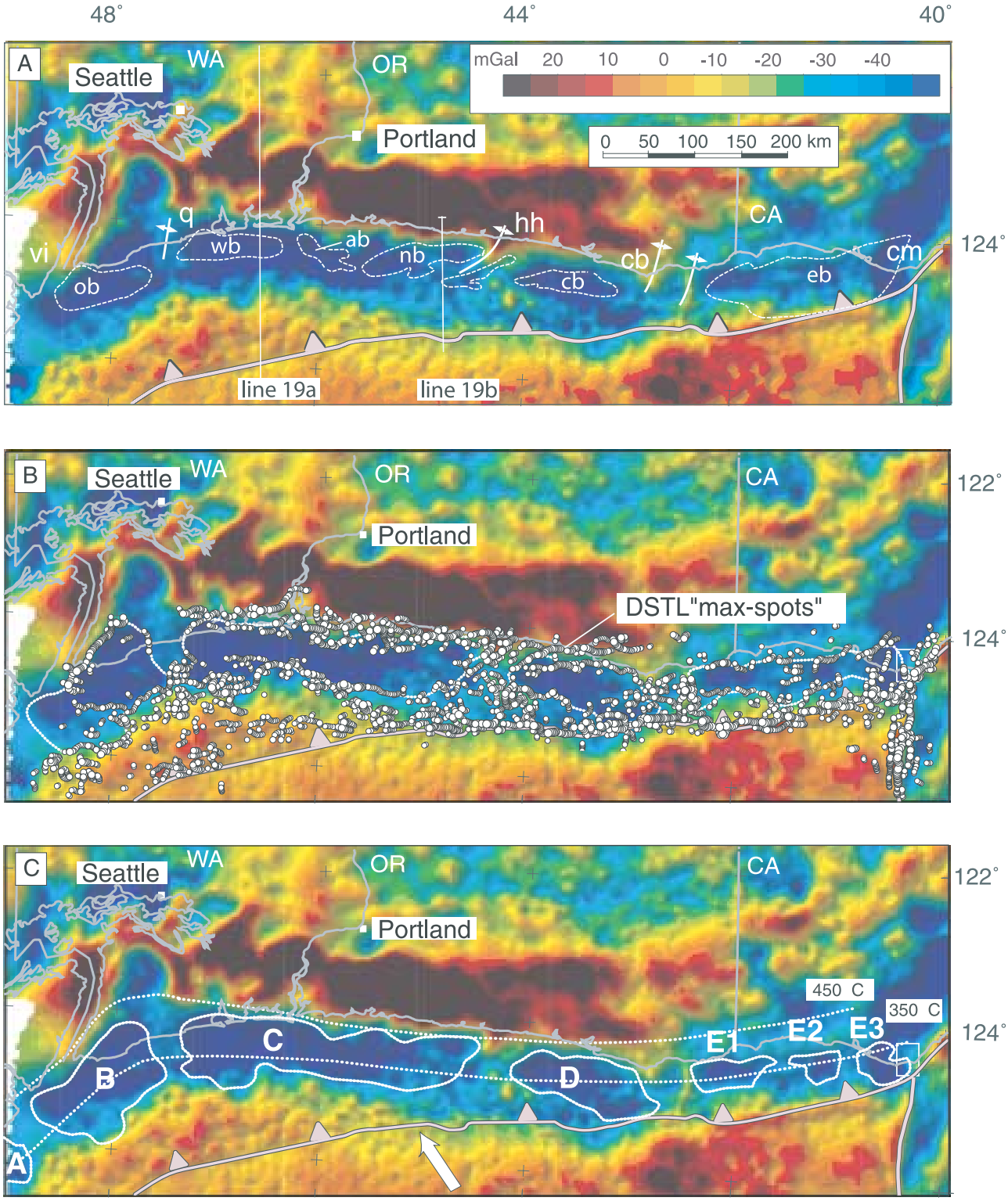


**Figure 18.** (a) Cascadia forearc basins, transverse uplifts, locked, and transition zones [*Oleskevich et al.*, 1999] on isostatic residual gravity, northwest United States, and Canada. Ob, wb, ab, nb, cb, eb are Olympic, Willapa, Astoria, Newport, Coos Bay, and Eel River basins, respectively; vi, q, hh, cb, and cm are Vancouver Island, Quinault, Heceta Head, Cape Blanco, and Cape Mendocino, respectively [*Snavely*, 1987; *Clarke*, 1992; *McNeill et al.*, 1998, 2000; *McCrory et al.*, 2002]. Segmentation due to transverse folds (white anticline symbols) is similar in scale to SW Japan. (b) Computer-generated gradients along margins of offshore gravity lows (circles) and interpreted boundaries (dotted line). (c) Offshore gravity lows indicating filled basins and accreted sediments (A–E) are interpreted to mark long-term asperities on the plate boundary based on correlation of similar features with high slip in Japan, Chile, and elsewhere (see text). Gradient along inboard basin margin is inferred downdip limit of large coseismic slip, consistent with geodetic and thermal data.

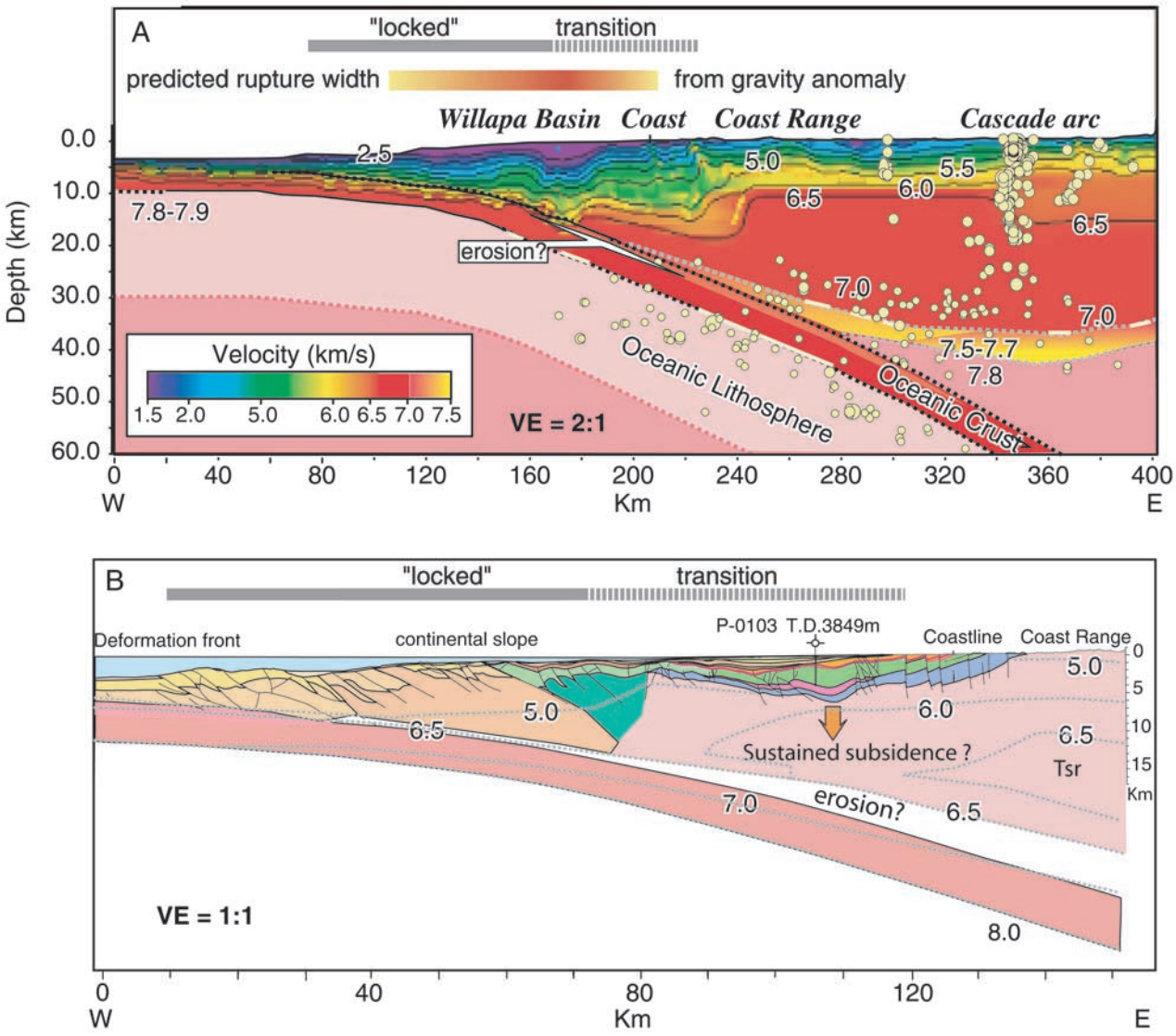


**Figure 19.** Seismic velocity cross sections of Cascadia convergent margin. (a) southwestern Washington, modified from *Parsons et al.* [1998]. Forearc gravity low coincides with velocity low of Willapa basin and thick sedimentary prism resting on wedge of higher velocity forearc crust. (b) Central Oregon, modified from *Snavely et al.* [1980] and *Trehu et al.* [1994]. Oligocene (green), Miocene (orange), and Plio-Pleistocene (yellow) shelf strata overlying thinned Eocene basalt basement (Tsr) in Newport basin may record sustained subsidence above subduction zone.

and northern Oregon, where there is good paleoseismic evidence for repeated coastal subsidence in great earthquakes [*Atwater and Hemphill-Haley*, 1997]. The basin-centered gravity lows straddle the 350°C isotherm on the plate boundary, and their inboard edges lie just off the coast, except in northwestern Washington, where they come onshore. If the forearc gravity lows of Cascadia are proxies for long-term coseismic slip distribution, then large slip in great earthquakes might be expected to occur offshore and drop off rapidly at the coast, with the largest asperity off Washington and northern Oregon. These conclusions are reasonably consistent with those made from contemporary measures of strain, given the uncertainties in our results and those inherent in elastic dislocation modeling of future ruptures [*Hyndman and Wang*, 1995a; *Savage et al.*, 2000; *McCaffrey et al.*, 2000].

[49] Cascadia may also exhibit rupture mode diversity. Abrupt coseismic subsidence has preserved prehistoric coastal marshes along much of the Cascadia margin, thus recording a paleohistory of subduction zone earthquakes from Vancouver Island to Cape Mendocino (Figure 20) [*Atwater and Hemphill-Haley*, 1997; *Nelson et al.*, 1996; *Clarke and Carver*, 1992; *Kelsey et al.*, 2002]. High-resolution chronology of the most recent subsidence event, along with the tsunami evidence from Japan, are consistent with a $M_w \sim 9$ rupture of the entire plate boundary in 1700 A.D. *Goldfinger et al.* [2003] have argued that similar great earthquakes are characteristic of Cascadia, occurring

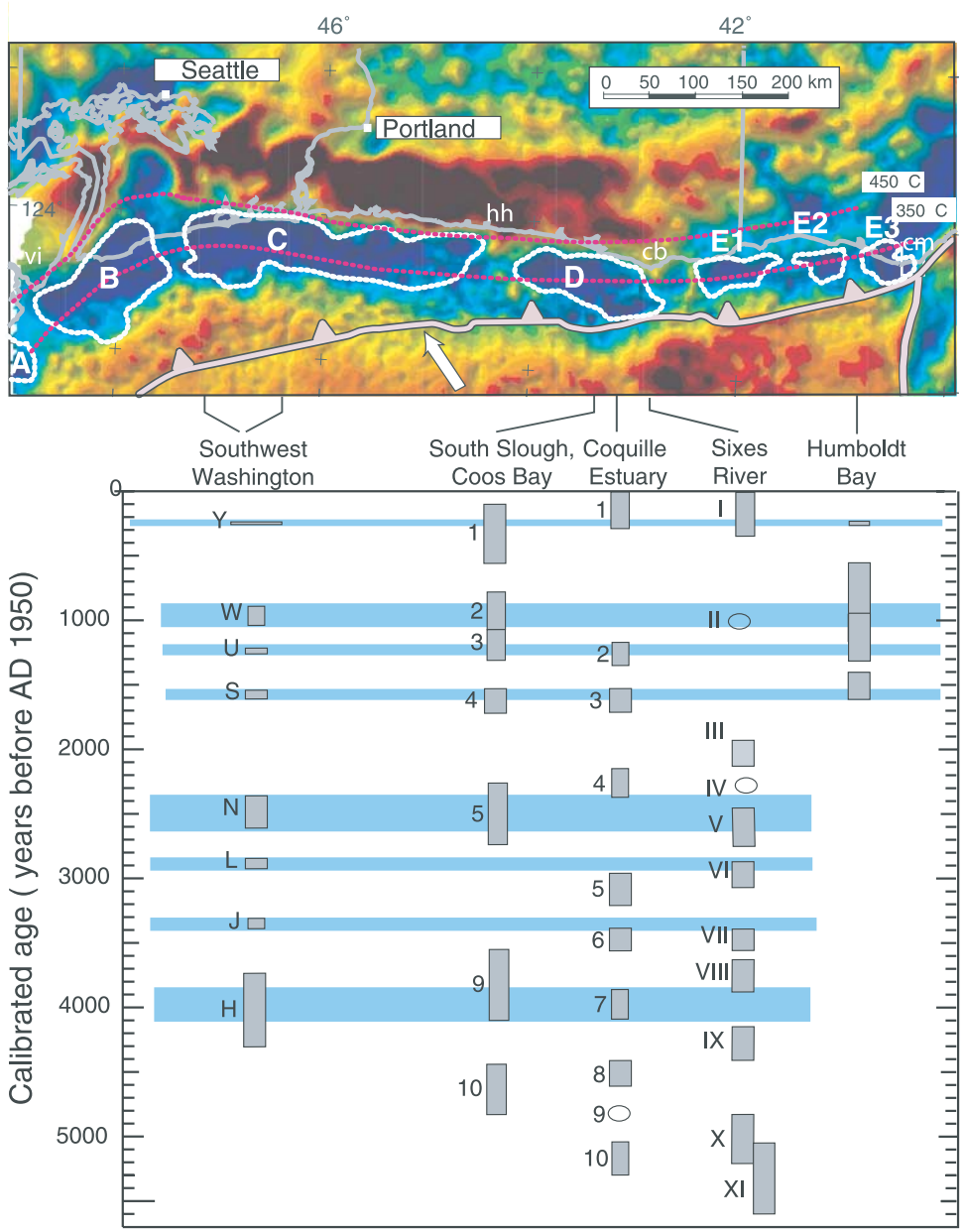


**Figure 20.** Paleoseismic record of Cascadia subduction earthquakes. Buried plant communities and peat deposits dated by $^{14}C$ record maximum ages of episodic coseismic subsidence in coastal estuaries, modified from *Kelsey et al.* [2002], *Nelson et al.* [1996], and *Clarke and Carver* [1992]. Y is 1700 A.D. event; horizontal lines indicate one possible correlation of events, using southwestern Washington sequence [*Atwater and Hemphill-Haley*, 1997] as reference (ovals are undated events). Uncorrelated earthquakes suggest rupture mode diversity [*Kelsey et al.*, 2002], consistent with large-scale asperities inferred from gravity lows.

on average, every 600 years, based on an equal number of post-Mazama-ash turbidites occurring in widely spaced submarine canyons along the Cascadia margin (13 turbidites in 7600 years). However, the coastal record of earthquakes prior to 1700 indicates that some earthquake-generated subsidence events south of Heceta Head are not observed to the north, and vice versa [*Nelson et al.*, 1996; *Kelsey et al.*, 2002]. The evidence for rupture mode diversity is consistent with structural segmentation of the margin proposed by *Nelson and Personius* [1996] and indicated by the large gravity lows and bounding transverse highs offshore. The existence of at least three major segments, Vancouver Island to Heceta Head, Heceta Head to Cape Blanco, and Cape Blanco to Cape Mendocino (Figure 20), suggests that a variety of large earthquakes are possible.

## 6. Conclusions

[50] In 29 of the largest twentieth century Circum-Pacific megathrust earthquakes, areas of high coseismic slip or

moment release, as determined from published waveform inversions, are focused beneath forearc structural lows revealed by satellite gravity, bathymetry, and marine geophysical studies. Coseismic slip is generally focused beneath the DSTL and its basins, which are underlain by a wedge of relatively high-velocity arc or continental crust. Seventy-nine percent of the asperity area, on average, lies beneath the DSTL, even though the DSTL occupies only 41% of the seismogenic zone defined by the maximum downdip limit of coseismic slip. Along the Nankai Trough of SW Japan, the steep gravity gradient marking the landward edge of the slope basins coincides with the 350°C isotherm on the plate boundary, presumably the downdip limit to unstable sliding. Slip maxima in the 1923, 1944, 1946, and 1968 earthquakes along the Nankai subduction zone were focused beneath five forearc basins, and the presently locked Tokai asperity is centered on a sixth. Coseismic slip beneath basins is also observed along the Aleutian, Mexico, Peru, and Chile subduction zones. This behavior appears typical of the subduction zones, requiring no special characteristics of the incoming plate or the forearc, although it may be enhanced by seamount and ridge subduction. The along-strike segmentation of the source zone into basins and ridges is commonly accomplished by strain partitioning due to oblique subduction or by the subduction of major fracture zones or ridges.

[51] The statistically significant focusing of slip beneath forearc basins appears unlikely to be the result of systematic bias in the slip inversions, which include tsunami, seismic, and geodetic inversions. More likely, there is a physical link between basin geometry and the slip process. In a majority of the subduction zones we examined, there is geologic evidence for sustained subsidence of the deep-sea terrace and its basins above the source zone in late Cenozoic time. The subsidence has commonly been attributed to subduction erosion. On a large scale, the coincidence of seismogenesis, subsidence, and subduction erosion implies a long-term relationship between seismic slip and basinal structure, with permanent interseismic subsidence aided by basal subduction erosion. Rupture mode diversity and dynamic interactions among asperities are not precluded by this model.

[52] Basin geometry may thus be a useful indicator of long-term seismic moment release in some subduction zones. In the source zone of the $M_w \sim 9$ great Cascadia earthquake of 1700 A.D., five very large basin-centered gravity lows lie within the locked and transition zones inferred from limited geodetic data. They may indicate where the 1700 A.D. asperities occurred at depth. If so, the margin appears to be seismically segmented and likely to produce rupture mode diversity. The shape of the forearc lows suggests that greater slip is likely beneath the Washington segment, perhaps extending beneath the coastline of the northwest Olympic Peninsula.

[53] **Acknowledgments.** We thank Wayne Thatcher, Roland von Huene, Heidi Houston, and an anonymous reviewer for thoughtful and constructive reviews. Our ideas were shaped by discussions with many colleagues over the years. Dave Engebretson, Al Lindh, Kelin Wang, and Sean Willett helped to clarify our thinking. We especially thank Kenji Satake and the National Institute of Advanced Industrial Science and Technology, Geological Survey of Japan for the opportunity to explore these issues while the first author was visiting the GSJ.

## References

Ando, M., Source mechanics and tectonic significance of historical earthquakes along the Nankai Trough, *Tectonophysics*, *27*, 119–140, 1975.

Atwater, B. F., and E. Hemphill-Haley, Recurrence intervals for great earthquakes of the past 3500 years at northeastern Willapa Bay, Washington, *U.S. Geol. Surv. Prof. Pap.*, *1576*, 108, 1997.

Azúa, B. M., C. DeMets, and T. Masterlark, Strong interseismic coupling, fault afterslip, and viscoelastic flow before and after the Oct. 9, 1995 Colima-Jalisco earthquake: Continuous GPS measurements from Colima, Mexico, *Geophys. Res. Lett.*, *29*(8), 1281, doi:10.1029/2002GL014702, 2002.

Bangs, N. L., and S. C. Cande, Episodic development of a convergent margin inferred from structures and processes along the southern Chile margin, *Tectonics*, *16*, 489–503, 1997.

Barrientos, S. E., Slip distribution of the 1985 central Chile earthquake, *Tectonophysics*, *145*, 225–241, 1988.

Barrientos, S. E., and S. N. Ward, The 1960 Chile earthquake: Inversion for slip distribution from surface deformation, *Geophys. J. Int.*, *103*, 589–598, 1990.

Beck, S. L., and D. H. Christensen, Rupture process of the February 4, 1965, Rat Islands earthquake, *J. Geophys. Res.*, *96*(B2), 2205–2221, 1991.

Beck, S. L., and L. J. Ruff, Rupture process of the great 1963 Kurile Islands earthquake sequence: Asperity interaction and multiple event rupture, *J. Geophys. Res.*, *92*, 14,123–14,138, 1987.

Blakely, R. J., and R. W. Simpson, Approximating edges of source bodies from magnetic and gravity anomalies, *Geophysics*, *51*, 1494–1498, 1986.

Boyd, T. M., E. R. Engdahl, and W. Spence, Seismic cycles along the Aleutian arc: Analysis of seismicity from 1957 through 1991, *J. Geophys. Res.*, *100*(B1), 621–644, 1995.

Brocher, T. M., G. S. Fuis, M. A. Fisher, G. Plafker, M. J. Moses, J. Taber, and N. I. Christensen, Mapping the megathrusts beneath the northern Gulf of Alaska using wide-angle seismic data, *J. Geophys. Res.*, *99*(B6), 11,663–11,686, 1994.

Bruns, T. R., R. von Huene, and R. C. Culotta, Geology and petroleum potential of the Shumagin margin, Alaska, in *Geology and Resource Potential of the Continental Margin of Western North America and Adjacent Ocean Basins-Beaufort Sea to Baja California*, *Earth Sci. Ser.*, vol. 6, edited by D. W. Scholl, A. Grantz, and J. G. Vedder, pp. 157–190, Circum-Pac. Counc. for Energy and Miner. Resour., Houston, Tex., 1987.

Byrne, D. E., D. M. Davis, and L. R. Sykes, Loci and maximum size of thrust earthquakes and the mechanics of the shallow region of subduction zones, *Tectonics*, *7*, 833–857, 1988.

Christensen, D. H., and S. L. Beck, The rupture process and tectonic implications of the great 1964 Prince William Sound earthquake, *Pure Appl. Geophys.*, *142*(1), 29–53, 1994.

Cifuentes, I. L., The 1960 Chilean earthquake, *J. Geophys. Res.*, *94*(B1), 665–680, 1989.

Clarke, S. H., Geology of the Eel River basin and adjacent region: Implications for late Cenozoic tectonics of the southern Cascadia subduction zone and Mendocino triple junction, *AAPG Bull.*, *76*, 199–224, 1992.

Clarke, S. H., and G. A. Carver, Late Holocene tectonics and paleoseismicity, southern Cascadia subduction zone, *Science*, *255*(5041), 188–192, 1992.

Cloos, M., Thrust-type subduction-zone earthquakes and seamount asperities: A physical model for seismic rupture, *Geology*, *20*, 601–604, 1992.

Cloos, M., and R. L. Shreve, Shear-zone thickness and the seismicity of Chilean- and Mariana-type subduction zones, *Geology*, *24*, 107–110, 1994.

Collot, J.-Y., P. Charvis, M.-A. Gutscher, and S. Operto, Exploring the Ecuador-Colombia active margin and interplate seismogenic zone, *Eos Trans. AGU*, *83*, 185, 189–190, 2002.

Compte, D., A. Eisenberg, E. Lorca, M. Pardo, L. Ponce, R. Saragoni, S. K. Singh, and G. Suarez, The great 1985 central Chile earthquake: A repeat of previous great earthquakes in the region?, *Science*, *233*, 449–453, 1986.

Das, S., and B. V. Kostrov, Inversion for slip rate history and distribution with stabilizing constraints: Application to the 1986 Andreanof Islands earthquake, *J. Geophys. Res.*, *95*, 6899–6913, 1990.

Dickinson, W. R., Forearc basins, in *Tectonics of Sedimentary Basins*, edited by C. J. Busby and R. V. Ingersoll, pp. 221–261, Blackwell Sci., Malden, Mass., 1995.

Eastabrook, C. H., K. H. Jacob, and L. R. Sykes, Body wave and surface wave analysis of large and great earthquakes along the eastern Aleutian arc, 1923–1993: Implications for future events, *J. Geophys. Res.*, *99*(B6), 11,643–11,662, 1994.

Finn, C., G. Kimura, and K. Suyehiro, Introduction to the special section northeast Japan: A case history of subduction, *J. Geophys. Res.*, *99*(B11), 22,137–22,145, 1994.

Fisher, M., R. L. Detterman, and L. B. Magoon, Tectonics and petroleum geology of the Cook-Shelikof basin, southern Alaska, in *Geology and Resource Potential of the Continental Margin of Western North America and Adjacent Ocean Basins—Beaufort Sea to Baja California*, *Earth Sci. Ser.*, vol. 6, edited by D. W. Scholl, A. Grantz, and J. G. Vedder, pp. 213–228, Circum-Pac. Counc. for Energy and Miner. Resour., Houston, Tex., 1987.

Flueh, E. R., N. Vidal, C. R. Ranero, A. Hojka, R. von Huene, J. Bialas, K. Hinz, D. Cordoba, J. J. Danobeitia, and C. Zelt, Seismic investigation of the continental margin off- and onshore Valparaiso, Chile, *Tectonophysics*, *288*, 251–263, 1998.

Freymueller, J., and J. Beavan, Absence of strain accumulation in the western Shumagin segment of the Alaska subduction zone, *Geophys. Res. Lett.*, *26*(21), 3233–3336, 1999.

Freymueller, J. T., S. C. Cohen, and H. J. Fletcher, Spatial variations in present-day deformation, Kenai Peninsula, Alaska, and their implications, *J. Geophys. Res.*, *105*(B4), 8079–8101, 2000.

Fryer, G. J., and P. Watts, Motion of the Ugamak Slide, probable source of the tsunami of 1 April 1946, Proceedings of the International Tsunami Symposium 2001, pp. 683–694, NOAA Pac. Mar. Environ. Lab., Seattle, 2001.

Geist, E. L., and D. W. Scholl, Large-scale deformation related to the collision of the Aleutian Arc with Kamchatka, *Tectonics*, *13*, 538–560, 1994.

Geist, E. L., J. R. Childs, and D. W. Scholl, The origin of summit basins of the Aleutian Ridge: Implications for block rotation of an arc massif, *Tectonics*, *7*, 327–341, 1988.

Goldfinger, C., C. H. Nelson, and J. E. Johnson, Holocene earthquake records from the Cascadia subduction zone and northern San Andreas fault based on precise dating of offshore turbidities, *Annu. Rev. Earth Planet. Sci.*, *31*, 555–577, 2003.

Gorbatov, A., V. Kostoglodov, G. Suarez, and E. Gordeev, Seismicity and structure of the Kamchatka subduction zone, *J. Geophys. Res.*, *102*(B8), 17,883–17,898, 1997.

Hartzell, S., and C. Langer, Importance of model parameterization in finite fault inversions: Application to the 1974 $M_w$ 8.0 Peru earthquake, *J. Geophys. Res.*, *98*(B12), 22,123–22,134, 1993.

Hirata, K., E. Geist, K. Satake, Y. Tanioka, and S. Yamaki, Slip distribution of the 1952 Tokachi-Oki earthquake (*M* 8.1) along the Kuril trench deduced from tsunami waveform inversion, *J. Geophys.*, *108*(B4), 2196, doi:10.1029/2002JB001976, 2003.

Holbrook, W. S., D. Lizarralde, S. McGeary, N. Bangs, and J. Diebold, Structure and composition of the Aleutian arc and implications for continental crustal growth, *Geology*, *27*, 31–34, 1999.

Holdahl, S. R., and J. Sauber, Coseismic slip in the 1964 Prince William Sound earthquake: A new geodetic inversion, *Pure Appl. Geophys.*, *142*(1), 55–82, 1994.

Houston, H., and E. R. Engdahl, A comparison of the spatio-temporal distribution of moment release for the 1986 Andreanof Islands earthquake with relocated seismicity, *Geophys. Res. Lett.*, *16*(12), 1421–1424, 1989.

Hyndman, R. D., and K. Wang, The rupture zone of Cascadia great earthquakes from current deformation and the thermal regime, *J. Geophys. Res.*, *100*(B11), 22,133–22,154, 1995a.

Hyndman, R. D., and K. Wang, Thermal constraints on the seismogenic portion of the southwestern Japan subduction thrust, *J. Geophys. Res.*, *100*(B8), 15,373–15,392, 1995b.

Ishibashi, K., and K. Satake, Problems on forecasting great earthquakes in the subduction zones around Japan by means of paleoseismology (in Japanese) (Appendix), *J. Seismol. Soc. Jpn.*, *50*, 1–21, 1998.

Johnson, J. M., and K. Satake, Rupture extent of the 1938 Alaskan earthquake as inferred from tsunami waveforms, *Geophys. Res. Lett.*, *21*(8), 733–736, 1994.

Johnson, J. M., and K. Satake, The 1965 Rat Islands earthquake: A critical comparison of seismic and tsunami wave inversions, *Bull. Seismol. Soc. Am.*, *86*, 1229–1237, 1996.

Johnson, J. M., and K. Satake, Estimation of seismic moment and slip distribution of the April 1, 1946, Aleutian tsunami earthquake, *J. Geophys. Res.*, *102*(B11), 11,765–11,774, 1997.

Johnson, J. M., and K. Satake, Asperity distribution of the 1952 great Kamchatka earthquake and its relation to future earthquake potential in Kamchatka, *Pure Appl. Geophys.*, *154*, 541–553, 1999.

Johnson, J. M., Y. Tanioka, L. J. Ruff, K. Satake, H. Kanamori, and L. R. Sykes, The 1957 great Aleutian earthquake, *Pure Appl. Geophys.*, *142*(1), 3–28, 1994.

Johnson, J. M., K. Satake, S. R. Holdahl, and J. Sauber, The 1964 Prince William Sound earthquake: Joint inversion of tsunami and geodetic data, *J. Geophys. Res.*, *101*(B1), 523–532, 1996.

Kelsey, H. M., D. C. Engebretson, C. E. Mitchell, and R. Ticknor, Topographic form of the coast ranges of the Cascadia margin in relation to coastal uplift rates and plate subduction, *J. Geophys. Res.*, *99*, 12,245–12,255, 1994.

Kelsey, H. M., R. C. Witter, and E. Hemphill-Haley, Plate-boundary earthquakes and tsunamis of the past 5500 yr, Sixes River estuary, southern Oregon, *Geol. Soc. Am. Bull.*, *114*, 298–314, 2002.

Khutorskoy, M. D., L. A. Delgado-Argote, R. Fernandez, V. I. Konov, and B. G. Polyak, Tectonics of the offshore Manzanillo and Tecpan basins, Mexican Pacific, from heat flow, bathymetric, and seismic data, *Geofis. Int.*, *33*, 161–185, 1994.

Kikuchi, M., and Y. Fukao, Iterative deconvolution of complex body waves from great earthquakes: The Tokachi-Oki earthquake of 1968, *Phys. Earth Planet. Inter.*, *37*(4), 235–248, 1985.

Kikuchi, M., and Y. Yamanaka, Rupture process of past large earthquakes and identification of asperities (in Japanese), *Seismo*, *5*, 6–7, 2001.

Kikuchi, M., M. Nakamura, and K. Yoshikawa, Source rupture processes of the 1944 Tonankai earthquake and the 1945 Mikawa earthquake derived from low-gain seismograms, *Earth Planets Space*, *55*, 159–172, 2003.

Klaeschen, D., I. Belykh, H. Gnibidenko, S. Patrikeyev, and R. von Huene, Structure of the Kuril Trench from seismic reflection records, *J. Geophys. Res.*, *99*(B12), 24,173–24,188, 1994.

Kodaira, S., N. Takahashi, J. Park, K. Mochizuki, M. Shinohara, and S. Kimura, Western Nankai Trough seismogenic zone: Results from a wide-angle ocean bottom seismic survey, *J. Geophys. Res.*, *105*(B3), 5887–5905, 2000.

Laursen, J., D. W. Scholl, and R. von Huene, Neotectonic deformation of the central Chile margin: Deepwater forearc basin formation in response to hot spot ridge and seamount subduction, *Tectonics*, *21*(5), 1038, doi:10.1029/2001TC901023, 2002.

Lay, T., and H. Kanamori, An asperity model of great earthquake sequences, in *Earthquake Prediction: An International Review*, *Maurice Ewing Ser.*, vol. 4, edited by D. Simpson and P. Richards, pp. 579–592, AGU, Washington, D.C., 1981.

Lepinay, M. B., et al., Large Neogene subsidence event along the middle America Trench off Mexico (18 degrees–19 degrees N): Evidence from submersible observations, *Geology*, *25*, 387–390, 1997.

Lisowski, M., J. C. Savage, W. H. Prescott, and W. K. Gross, Absence of strain accumulation in the Shumagin seismic gap, Alaska, 1980–1987, *J. Geophys. Res.*, *93*(B7), 7909–7922, 1988.

Mazzotti, S., X. L. Pichon, P. Henry, and S. I. Miyazaki, Full interseismic locking of the Nankai and Japan-west Kurile subduction zones: An analysis of uniform elastic strain accumulation in Japan constrained by permanent GPS, *J. Geophys. Res.*, *105*(B6), 13,159–13,178, 2000.

McCaffrey, R. M., Global variability in subduction thrust zone-forearc systems, *Pure Appl. Geophys.*, *142*, 173–224, 1993.

McCaffrey, R. M., D. Long, C. Goldfinger, P. C. Zwick, J. L. Nabelek, C. K. Johnson, and C. Smith, Rotation and plate locking along the southern Cascadia subduction zone, *Geophys. Res. Lett.*, *27*, 3117–3120, 2000.

McCrory, P. A., D. S. Foster, W. W. Danforth, and M. R. Hamer, Crustal deformation at the leading edge of the Oregon coast range block, offshore Washington (Columbia River to Hoh River), *U.S. Geol. Surv. Prof. Pap.*, *1661-A*, 47, 2002.

McNeill, L., C. Goldfinger, R. S. Yeats, and L. D. Kulm, in *Coastal Tectonics*, edited by I. S. Stewart and C. Vita-Finzi, *Geol. Soc. Spec. Publ.*, *146*, 321–342, 1998.

McNeill, L. C., C. Goldfinger, L. D. Kulm, and R. S. Yeats, Tectonics of the Neogene Cascadia forearc basin: Investigations of a deformed late Miocene unconformity, *Geol. Soc. Am. Bull.*, *112*(8), 1209–1224, 2000.

Mendoza, C., Coseismic slip of two large Mexican earthquakes from teleseismic body waveforms: Implications for asperity interaction in the Michoacan plate boundary segment, *J. Geophys. Res.*, *98*(B5), 8197–8210, 1993.

Mendoza, C., and S. H. Hartzell, Slip distribution of the 19 September 1985 Michoacan, Mexico earthquake: Near source and teleseismic constraints, *Bull. Seismol. Soc. Am.*, *79*, 655–699, 1989.

Mendoza, C., S. Hartzel, and T. Monfret, Wide-band analysis of the 3 March 1985 central Chile earthquake: Overall source process and rupture history, *Bull. Seismol. Soc. Am.*, *84*, 269–283, 1994.

Mogi, K., Relationship between the occurrence of great earthquakes and tectonic structures, *Bull. Earthquake Res. Inst. Univ. Tokyo*, *47*, 429–451, 1969.

Mordojovich, C., Sedimentary basins of Chilean Pacific offshore, *AAPG Stud. Geol.*, *12*, 63–82, 1981.

Mori, J., and K. Shimazaki, Inversion of intermediate-period Rayleigh waves for source characteristics of the 1968 Tokachi-Oki earthquake, *J. Geophys. Res.*, *90*, 11,374–11,382, 1985.

Nakanishi, A., N. Takahashi, J.-O. Park, S. Miura, S. Kodaira, Y. Kaneda, N. Hirata, T. Iwasaki, and M. Nakamura, Crustal structure across the coseismic rupture zone of the 1944 Tonankai earthquake, the central Nankai Trough seismogenic zone, *J. Geophys. Res.*, *107*(B1), 2007, doi:10.1029/2001JB000424, 2002.

Nakayama, W., and M. Takeo, Slip history of the 1994 Sanriku-Haruka-Oki, Japan earthquake deduced from strong-motion data, *Bull. Seismol. Soc. Am.*, *87*, 918–931, 1997.

Nelson, A. R., and S. F. Personius, The potential for great earthquakes in Oregon and Washington—An overview of recent coastal geologic studies and their bearing on segmentation of Holocene ruptures, central Cascadia subduction zone, in *Earthquake Hazards in the Pacific Northwest of the United States*, edited by A. M. Rogers et al., *U.S. Geol. Surv. Prof. Pap.*, *1560*, 91–114, 1996.

Nelson, A. R., I. Shennan, and A. J. Long, Identifying coseismic subsidence in tidal-wetland stratigraphic sequences at the Cascadia subduction zone of western North America, *J. Geophys. Res.*, *101*(3), 6115–6135, 1996.

Oleskevich, D. A., R. D. Hyndman, and K. Wang, The updip and down-dip limits to great subduction earthquakes: Thermal and structural models of Cascadia, South Alaska, SW Japan, and Chile, *J. Geophys. Res.*, *104*, 14,965–14,992, 1999.

Park, J.-O., T. Tsuru, S. Kodaira, P. R. Cummins, and Y. Kaneda, Splay fault branching along the Nankai subduction zone, *Science*, *297*, 1157–1160, 2002.

Parsons, T., A. M. Trehu, J. H. Luetgert, K. Miller, F. Kilbride, R. E. Wells, M. A. Fisher, E. Flueh, U. S. ten Brink, and N. I. Christensen, A new view into the Cascadia subduction zone and volcanic arc: Implications for earthquake hazards along the Washington margin, *Geology*, *26*, 199–202, 1998.

Plafker, G., Alaskan earthquake of 1964 and Chilean earthquake of 1960: Implications for arc tectonics, *J. Geophys. Res.*, *77*, 901–925, 1972.

Plafker, G., Regional geology and petroleum potential of the northern Gulf of Alaska continental margin, in *Geology and Resource Potential of the Continental Margin of Western North America and Adjacent Ocean Basins-Beaufort Sea to Baja California*, *Earth Sci. Ser.*, vol. 6, edited by D. W. Scholl, A. Grantz, and J. G. Vedder, pp. 229–268, Circum-Pac. Counc. for Energy and Miner. Resour., Houston, Tex., 1987.

Plafker, G., J. C. Moore, and G. R. Winkler, Geology of the southern Alaska Margin, in *The Geology of North America*, vol. G-1, *The Geology of Alaska*, edited by G. Plafker and H. C. Berg, pp. 389–449, Geol. Soc. of Am., Boulder, Colo., 1994.

Plafker, G., C. Synolakis, and E. Okal, New near-source Tsunami field data for the April 1, 1946 Aleutian earthquake, Alaska, *Eos Trans. AGU*, *82*(47), Fall Meet. Suppl., Abstract 5128–0603, 2001.

Ranero, C. R., and R. von Huene, Subduction erosion along the middle America convergent margin, *Nature*, *404*, 748–752, 2000.

Ruff, L., Do trench sediments affect great earthquake occurrence in subduction zones?, *Pure Appl. Geophys.*, *129*(1/2), 263–282, 1989.

Ruff, L. J., and A. D. Miller, Rupture process of large earthquakes in the northern Mexico subduction zone, *Pure Appl. Geophys.*, *142*(1), 101–171, 1994.

Ruff, L. J., and B. W. Tichelaar, What controls the seismogenic plate interface in subduction zones?, in *Subduction Top to Bottom*, *Geophys. Monogr. Ser.*, vol. 96, edited by G. E. Bebout et al., pp. 105–112, AGU, Washington, D.C., 1996.

Ryan, H. F., and D. W. Scholl, Geologic implications of great interplate earthquakes along the Aleutian arc, *J. Geophys. Res.*, *98*(B12), 22,135–22,146, 1993.

Sagiya, T., Interplate coupling in the Tokai District, central Japan, deduced from continuous GPS data, *Geophys. Res. Lett.*, *26*, 15, 2315–2318, 1999.

Sagiya, T., and W. Thatcher, Coseismic slip resolution along a plate boundary megathrust: The Nankai Trough, southwest Japan, *J. Geophys. Res.*, *104*(B1), 1111–1129, 1999.

Sagiya, T., S. Miyazaki, and T. Tada, Continuous GPS array and present-day crustal deformation of Japan, *Pure Appl. Geophys.*, *157*(11–12), 2303–2322, 2000.

Satake, K., Inversion of tsunami waveforms for the estimation of heterogeneous fault motion of large submarine earthquakes: The 1968 Tokachi-Oki and 1983 Japan Sea earthquakes, *J. Geophys. Res.*, *94*, 5627–5636, 1989.

Satake, K., Depth distribution of coseismic slip along the Nankai Trough, Japan, from joint inversion of geodetic and tsunami data, *J. Geophys. Res.*, *98*, 4553–4565, 1993.

Satake, K., and K. Wang, Coseismic fault slip and seismic moment of the 1700 Cascadia earthquake estimated from Japanese tsunami observations, in Penrose Conference 2000, great Cascadia earthquake tricentennial, *Spec. Pap. Oreg. Dep. Geol. Miner. Ind.*, *33*, 110–111, 2000.

Satake, K., K. Shimazaki, Y. Tsuji, and K. Ueda, Time and size of a giant earthquake in Cascadia inferred from Japanese tsunami records of January 1700, *Nature*, *379*(6562), 246–249, 1996.

Savage, J. C., J. L. Svarc, W. H. Prescott, and M. H. Murray, Deformation across the forearc of the Cascadia subduction zone at Cape Blanco, Oregon, *J. Geophys. Res.*, *105*(B2), 3095–3102, 2000.

Scholl, D. W., and R. von Huene, Evolution of convergent margins—Impact of new and reassessed observations on rates of crustal recycling and arc magmatic additions, in *Margins Conference and Deutsche geologische gesellschaft (DGG) and Geologische Vereinigung (GV) Annual Meeting Programs and Abstracts*, edited by S. Roth and A. Ruggeberg, pp. 190–191, Christian Albrechts Univ., Kiel, 2001.

Scholl, D. W., R. von Huene, T. L. Vallier, and D. G. Howell, Sedimentary masses and concepts about tectonic processes at underthrust ocean margins, *Geology*, *8*, 564–568, 1980.

Scholl, D. W., T. L. Vallier, and A. J. Stevenson, Geologic evolution and petroleum geology of the Aleutian Ridge, in *Geology and Resource Potential of the Continental Margin of Western North America and Adjacent Ocean Basins-Beaufort Sea to Baja California*, *Earth Sci. Ser.*, vol. 6, edited by D. W. Scholl, A. Grantz, and J. G. Vedder, pp. 124–155, Circum-Pac. Counc. for Energy and Miner. Resour., Houston, Tex., 1987.

Scholl, D. W., R. von Huene, and H. F. Ryan, Basal subduction erosion and the formation of the Aleutian Terrace and underlying forearc basin, in *Program and Abstracts, 3rd Biennial Workshop on Subduction Processes Emphasizing the Kurile-Kamchatka-Aleutian Arc*, pp. 61–62, Geophys. Inst., Univ. of Alaska, Fairbanks, 2002.

Scholz, C. H., *The Mechanics of Earthquakes and Faulting*, 439 pp., Cambridge Univ. Press, New York, 1990.

Schwartz, S., and L. Ruff, The 1968 Tokachi-Oki and the 1969 Kurile Island earthquakes: Variability in the rupture process, *J. Geophys. Res.*, *90*, 8613–8626, 1985.

Schwartz, S., and L. Ruff, Asperity distribution and earthquake occurrence in the southern Kurile Islands arc, *Phys. Earth Planet. Inter.*, *49*(1–2), 54–77, 1987.

Schwartz, S. Y., Noncharacteristic behavior and complex recurrence of large subduction zone earthquakes, *J. Geophys. Res.*, *104*, 23,111–23,125, 1999.

Smith, W., and D. T. Sandwell, Global sea floor topography from satellite altimetry and ship depth soundings, *Science*, *277*(5334), 1956–1962, 1997.

Snavely, P. D., Jr., Tertiary geologic framework, neotectonics, and petroleum potential of the Oregon-Washington continental margin, in *Geology and Resource Potential of the Continental Margin of Western North America and Adjacent Ocean Basins-Beaufort Sea to Baja California*, *Earth Sci. Ser.*, vol. 6, edited by D. W. Scholl, A. Grantz, and J. G. Vedder, pp. 124–155, Circum-Pac. Counc. for Energy and Miner. Resour., Houston, Tex., 1987.

Snavely, P. D., Jr., H. C. Wagner, and D. L. Lander, Geologic cross section of the central Oregon continental margin, *Map and Chart Ser. MC-28J*, scale 1:250,000, Geol. Soc. of Am., Boulder, Colo., 1980.

Spence, W., C. Mendoza, E. R. Engdahl, G. L. Choy, and E. Norabuena, Seismic subduction of the Nazca Ridge as shown by the 1996–1997 Peru earthquakes, *Pure Appl. Geophys.*, *154*, 753–776, 1999.

Sugiyama, Y., Neotectonics of southwest Japan due to the right-oblique subduction of the Philippine Sea plate, *Geofis. Int.*, *33*(1), 53–76, 1994.

Swenson, J. L., and S. L. Beck, Source characteristics of the 12 November 1996 $M_w$ 7.7 Peru subduction zone earthquake, *Pure Appl. Geophys.*, *154*, 731–751, 1999.

Tanioka, Y., and F. I. Gonzalez, The Aleutian earthquake of June 10, 1996 ($M_w$ 7.9) ruptured parts of both the Andreanof and Delarof segments, *Geophys. Res. Lett.*, *25*(12), 2245–2248, 1998.

Tanioka, Y., and K. Satake, Coseismic slip distribution of the 1946 Nankai earthquake and aseismic slips caused by the earthquake, *Earth Planets Space*, *53*, 235–241, 2001a.

Tanioka, Y., and K. Satake, Detailed coseismic slip distribution of the 1944 Tonankai earthquake estimated from tsunami waveforms, *Geophys. Res. Lett.*, *28*, 1075–1078, 2001b.

Tanioka, Y., L. Ruff, and K. Satake, The Sanriku-Oki Japan earthquake of December 28, 1994 ($M_w$ 7.7): Rupture of a different asperity from a previous earthquake, *Geophys. Res. Lett.*, *23*, 1465–1468, 1996.

Thatcher, W., Order and diversity in the modes of Circum-Pacific earthquake recurrence, *J. Geophys. Res.*, *95*(B3), 2609–2623, 1990.

Tichelaar, B. W., and L. J. Ruff, Seismic coupling along the Chilean subduction zone, *J. Geophys. Res.*, *96*, 11,997–12,022, 1991.

Tichelaar, B. W., and L. J. Ruff, Depth of seismic coupling along subduction zones, *J. Geophys. Res.*, *98*, 2017–2037, 1993.

Trehu, A. M., I. Asudeh, T. M. Brocher, J. Leutgert, W. D. Mooney, J. N. Nabelek, and Y. Nakamura, Crustal architecture of the Cascadia fore arc, *Science*, *265*, 237–243, 1994.

Tsuru, T., J.-O. Park, N. Takahashi, S. Kodaira, Y. Kido, Y. Kaneda, and Y. Kono, Tectonic features of the Japan Trench convergent margin off Sanriku, northeastern Japan, revealed by multichannel seismic reflection data, *J. Geophys. Res.*, *105*(B7), 16,403–16,413, 2000.

Vallier, T. L., D. W. Scholl, M. A. Fisher, T. R. Bruns, F. H. Wilson, R. von Huene, and A. J. Stevenson, Geologic framework of the Aleutian

Arc, Alaska, in *The Geology of North America*, vol. G-1, *The Geology of Alaska*, edited by G. Plafker and H. C. Berg, pp. 367–388, Geol. Soc. of Am., Boulder, Colo., 1994.

von Huene, R., and D. Klaeschen, Opposing gradients of permanent strain in the aseismic zone and elastic strain across the seismogenic zone of the Kodiak shelf and slope, Alaska, *Tectonics*, *18*, 248–262, 1999.

von Huene, R., and S. Lallemand, Tectonic erosion along the Japan and Peru convergent margins, *Geol. Soc. Am. Bull.*, *102*, 704–720, 1990.

von Huene, R., and D. W. Scholl, Observations at convergent margins concerning sediment subduction, subduction erosion, and the growth of continental crust, *Rev. Geophys.*, *29*, 279–316, 1991.

von Huene, R., M. A. Fisher, and T. R. Bruns, Geology and evolution of the Kodiak margin, Gulf of Alaska, in *Geology and Resource Potential of the Continental Margin of Western North America and Adjacent Ocean Basins-Beaufort Sea to Baja California*, *Earth Sci. Ser.*, vol. 6, edited by D. W. Scholl, A. Grantz, and J. G. Vedder, pp. 124–155, Circum-Pac. Counc. for Energy and Miner. Resour., Houston, Tex., 1987.

von Huene, R., R. E. Suess, and Leg 112 Shipboard Scientists, Ocean Drilling Program Leg 112, Peru continental margin, part I, Tectonic history, *Geology*, *16*, 934–938, 1988.

von Huene, R., D. Klaeschen, and B. Cropp, Tectonic structure across the accretionary and erosional parts of the Japan Trench margin, *J. Geophys. Res.*, *99*(B11), 22,349–22,361, 1994.

von Huene, R., J. Corvalan, E. R. Flueh, K. Hinz, J. Korstgard, C. R. Ranero, and W. Weintrube, and CONDOR scientists, Tectonic control of the subducting Juan Fernandez Ridge on the Andean margin near Valparaiso, Chile, *Tectonics*, *16*, 474–488, 1997.

von Huene, R., D. Klaeschen, and J. Fruehn, Relation between the subducting plate and seismicity associated with the great 1964 Alaska earthquake, *Pure Appl. Geophys.*, *154*, 575–591, 1999.

Wald, D. J., and P. G. Somerville, Variable-slip rupture model of the great 1923 Kanto, Japan earthquake: Geodetic and body-waveform analysis, *Bull. Seismol. Soc. Am.*, *85*, 159–177, 1995.

Willett, S. D., Dynamic and kinematic growth and change of a Coulomb wedge, in *Thrust Tectonics*, edited by K. R. McClay, pp. 19–31, Chapman and Hall, New York, 1992.

Yagi, Y., M. Kikuchi, S. Yoshida, and Y. Yamanaka, Source process of the Hyuga-nada earthquake of April 1, 1968 (Mjma 7.5), and its relationship to subsequent sesimicity, *J. Seismol. Soc. Jpn.*, *2*(51), 139–148, 1998.

Yale, M. M., D. T. Sandwell, and A. T. Herring, What are the limitations of satellite altimetry?, *Leading Edge*, *17*, 73–76, 1998.

Zobin, V. M., The rupture history of the $M_w$ 8.0 Jalisco, Mexico earthquake of 1995 October 9, *Geophys. J. Int.*, *130*, 220–228, 1997.

Zweck, C., J. T. Freymueller, and S. C. Cohen, Three-dimensional elastic dislocation model of the post-seismic response to the 1964 Alaska earthquake, *J. Geophys. Res.*, *107*(B4), doi:10.1029/2001JB000409, 2002.

R. J. Blakely, U.S. Geological Survey, MS 989, 345 Middlefield Road, Menlo Park, CA 94025, USA. (blakely@usgs.gov)

P. A. Dinterman and R. E. Wells, U.S. Geological Survey, MS 973, 345 Middlefield Road, Menlo Park, CA 94025, USA. (rwells@usgs.gov)

D. W. Scholl, U.S. Geological Survey, MS 977, 345 Middlefield Road, Menlo Park, CA 94025, USA. (dscholl@usgs.gov)

Y. Sugiyama, Geological Survey of Japan, National Institute of Advanced Industrial Science and Technology, 1-1-3 Higashi, Tsukuba, Ibaraki 305-8567, Japan. (sugiyama-y@aist.go.jp)